Available online at www.sciencedirect.com
SCIENCE DIRECT
Computers and Structures 84 (2006) 657–675
Computers & Structures
www.elsevier.com/locate/compstruc

Accurate computation of critical local quantities in composite laminated plates under transverse loading

P.M. Mohite, C.S. Upadhyay *

Department of Aerospace Engineering, Indian Institute of Technology, Kanpur 208016, India

Received 3 June 2005; accepted 20 November 2005
Available online 3 February 2006

Abstract

The design of laminated composite based components requires a detailed analysis of the response of the structure when subjected to external loads. For the analysis of laminated composite plates, several plate theories have been proposed in the literature. Generally, these plate theories are used to obtain certain global response quantities like the buckling load. However, the use of these theories to obtain local response quantities, i.e. point-wise stresses; interlaminar stresses and strains, can lead to significant errors.

In this paper, a detailed study of the quality of the point-wise stresses obtained using higher-order shear deformable, hierarchic and layerwise theories is done for a plate under transverse loading. The effect of equilibrium based post-processing on the transverse stress quantities is also studied. From the detailed study it is observed that the layerwise theory is very accurate. However, for all the models proper mesh design is required to capture boundary layer effects, discretization error, etc. Using focussed adaptivity, and post-processed state of stress, accurate representation of the local state of stress can be obtained, even with the higher-order shear deformable theories. Using this approach, the first-ply failure load is obtained with the Tsai–Wu criterion. It is observed that use of an adaptive procedure leads to significantly lower failure loads as compared to those given in the literature.

Keywords: Plate models; HSDT; Hierarchic; Layerwise model; Transverse loading; Transverse deflection; Equilibrium approach; First-ply failure load; A posteriori error estimation; Focussed adaptivity; Point-wise stress; Composite laminates

1. Introduction

Thin layered (or laminated) structures made of composite laminates are increasingly used in the manufacture of structural components. The enhanced strength to weight ratios make composites especially attractive for aerospace applications. With an increasing demand to maximize payload carrying capabilities of aerial vehicles, shape and topology optimization of structural components has become an important thrust area. All the optimization problems posed in this context are constrained approximation problem with constraints on failure load, maximum transverse deflection, buckling load, natural frequency, etc. In order to obtain an acceptable optimally designed component, from a computational analysis, it becomes imperative to estimate the constraint quantities accurately, at each step of the design process.

One important aspect of the response of laminated structures that a designer considers is the onset of failure in a laminated structure. Onset of failure in composite laminated plates requires the local stress state to be known in the structure, particularly near structural details; at interlamina interface and in the individual lamina. Accurate prediction of the local stress state becomes important for a reliable estimate of the failure load, which may be crucial for a safe design of the component.

Analysis of thin laminated domains is generally done using dimensionally reduced plate models. Several plate theories have been proposed in the literature (see [1–22] for example). The goal is generally to give a higher-order

* Corresponding author.
E-mail address: shekhar@iitk.ac.in (C.S. Upadhyay).

0045-7949/$ - see front matter © 2005 Elsevier Ltd. All rights reserved.
doi:10.1016/j.compstruc.2005.11.004

representation of the transverse shear terms, as in [1–11]; or to design families of plate theories with guaranteed convergence to the three-dimensional solutions in some norm (see [13,14]). However, not much can be said about the accuracy of the local stress state and displacements. In general, for thin domains severe boundary layers and corner singularities may exist. Due to the presence of these, the stress "hot-spots" are likely to occur in the vicinity of boundaries and corners (see [25–30]). Resolution of these effects effectively, is essential in order to accurately obtain the desired local stress state. One of the goals of this study is to determine the quality of the local state of stress, obtained using various families of plate models commonly used in engineering practice. A detailed comparison will be done with respect to the exact three-dimensional elasticity solutions given in [37,38], for both symmetric and anti-symmetric stacking of the laminae. The values of the in-plane stresses obtained directly from the finite element computations will be compared to the three-dimensional elasticity solution. The effect of model order and in-plane approximation order, on the accuracy of these stresses will be demonstrated. For the transverse stress components, the values obtained from the finite element solution directly, and those obtained using the equilibrium approach of post-processing, will be compared to the exact ones. Another major goal of the study is to show that without proper mesh design, i.e. use of meshes obtained using an adaptive refinement procedure (which also resolves the boundary-layer effect and effect of singularities), the computed local stresses obtained by using the popular plate models, can be significantly different from the exact ones. Further, the study aims at clearly demonstrating the need for proper mesh design in the computation of critical failure loads.

Finally, this study aims to obtain reliable values of the first-ply failure load, using the available models, and compare them with those given in [42]. It will be demonstrated that depending on the applied boundary conditions, stacking sequence and ply orientation, the reliable values of the first-ply failure load can be significantly lower than those obtained using the commonly used meshes and polynomial approximations.

2. Plate models

2.1. Brief review

The system of partial differential equations of three-dimensional elasticity is generally intractable analytically, especially for a layered medium. The development of classical theories was motivated to alleviate these problems by reducing the dimension for analysis. For example, in case of plates and shells reduction from three to two dimension reduces the computational cost and enables the handling of a large class of problems.

In the following paragraphs we give a brief review of some of the plate theories used for homogeneous and laminated plates. Traditionally, for the plate and shell like thin structures, several plate theories have been proposed. These can be broadly classified as

(1) shear deformable theories;
(2) hierarchic plate theories and
(3) layer-by layer theories.

2.1.1. Shear deformable theories

These are essentially the variants of the classical plate theory. In the classical plate theory the displacement components have linear transverse representation. This theory does not take into account the transverse shear deformations and transverse normal stress. Reissner [1] and Mindlin [2] improved the classical theory by adding effects of transverse shear and influence of rotary inertia, shear on flexural motions, respectively. Further, Reissner [3,4] improved it by considering non-homogeneous construction of plate. The variants of Reissner–Mindlin theory are called *first-order shear deformable theories*.

The theories which were originally proposed for homogeneous isotropic plates were then applied for layered plates. Classical laminate theory is a direct application of classical plate theory to laminates. The classical laminate theory smears out the effect of individual lamina across the thickness direction of the laminate. In this theory it is assumed that the laminate is in plane stress state; the individual lamina are linear elastic and there is perfect bonding between the layers. As in classical plate theory, the transverse shear deformations and transverse normal stress is ignored.

Reissner and Stavsky [5] improved the classical laminate theory by adding bending and stretching coupling for unsymmetric laminates. Whitney and Pagano [6] further studied these laminates by adding shear and rotary effects. They found that the unsymmetrically laminated plates exhibit the same bending–extensional coupling phenomenon found in classical laminated plate theory based on Kirchhoff assumptions. Further, they found that the deflections of the plate are dependent upon the shear correction factor and inaccuracies in calculating stresses for low span to depth ratios are not alleviated. Whitney [7] attempted to give shear correction factors for orthotropic laminates under the action of static load using the procedure similar to given by Reissner [1].

When the transverse variation of the displacement components is represented by using polynomial of degree n then the model is called as nth-*order shear deformable theory* or *higher-order shear deformable theory* (HSDT). Whitney and Sun [8] have developed *second-order shear deformable theory* for laminated composites. The governing equations for the unsymmetrically laminated plates showed the coupling phenomenon between all of the deformation modes present in the theory. Further they observed improved results for extensional motion compared to earlier existing laminated plate theories.

Lo et al. gave a *third-order shear deformation theory* for the analysis of both homogeneous [9] and laminated [10] plates. This theory does not require the shear correction

factor. Reddy [11] proposed similar displacement field as in [9] and also imposed the condition of parabolic distribution of the transverse shear strains through thickness of the plate to satisfy the zero transverse shear stress on the top and bottom face of the plate.

2.1.2. Hierarchic plate theories

In these, the displacement components have a zig-zag or hierarchic representation through the thickness. The hierarchic plate models are a sequence of mathematical models, the exact solutions of which constitute a converging sequence of functions in an appropriate norm. The construction of hierarchic models for homogeneous isotropic plates and shells was given by Szabó and Sharmann [12] and later for laminated plates by Babuška et al. [13], and Szabó et al. [14]. The solutions of the lower order models are embedded in the highest order model and these models can be adapted according to the requirement.

In these models the displacement field is given as product of functions that depend upon the variables associated with the plate, plate middle surface, and functions of the transverse variable. The transverse functions are derived on the basis of the degree to which the equilibrium equations of three-dimensional elasticity are satisfied. The Fourier transform of the equations of motion is performed which results in two-point boundary value problems for the transverse functions. These are characterized by the geometric parameters and wave vector. These functions are expanded in powers of wave vector around zero. The transverse functions are obtained by solving equations obtained by substituting the expanded functions into the transformed form of equations of motion.

2.1.3. Layer-by-layer theories

In these theories, the individual lamina have continuous through thickness representation of displacements.

Srinivas [15] assumed the displacement field to be piecewise linear across the thickness. Also the effects of transverse shear deformations and rotary inertia are included.

Di Sciuva [16] assumed the displacement field to be piecewise linear for in-plane components while the transverse displacement is constant throughout the laminate thickness. Also the static and geometric continuity condition at the interface was enforced. The effects of shear and rotary inertia were also included in the formulation. Further, an anisotropic, multi-layered shear-deformable rectangular plate element was developed in [17]. This plate element was shown to be very efficient in predicting the response of thick and thin laminated plates.

Toledano and Murakami [18] proposed a model for arbitrary laminate configuration. The displacement field was as in Di Sciuva's model and continuity of interlaminar stresses was enforced. Since the transverse displacement is constant through laminate thickness, the transverse shear strains are constant in a layer but different in each layer. The shear stresses were assumed to be quadratic functions of the local thickness coordinates across each layer. The governing equations were derived using Reissner's new principle [19]. In all these theories no shear correction factor was applied.

Bhaskar and Vardan [20] proposed a model using piecewise displacement representation for symmetric laminates under unsymmetric loading. The transverse variation of the in-plane displacement components is represented by a polynomial of degree three multiplied by the Heaviside unit step function. The transverse displacement was given as a quadratic or higher-order variation with respect to the transverse coordinate. Also the zero shear condition on the free surfaces of the plate, displacement compatibility as well as transverse shear continuity at the interface was enforced.

Barbero and Reddy [21] proposed a model with piecewise smooth approximation of the displacement components. The transverse displacement is constant through the laminate thickness.

Ahmed and Basu [22] proposed a model in which all the displacement components are represented as product of in-plane and out-of-plane approximating functions of same order. The hierarchic approximating functions were used.

A more detailed survey of the plate theories used in literature is available in Kapania and Raciti [23] and Ugrimov [24].

2.2. Plate models in present study

The generic representation of the displacement field for the plate models is given as

$$\mathbf{u}(x,y,z) = \begin{Bmatrix} u(x,y,z) \\ v(x,y,z) \\ w(x,y,z) \end{Bmatrix} = [\phi(z)]\mathbf{U}(x,y) \tag{1}$$

where

$$[\phi(z)] = \begin{bmatrix} \phi_1(z) & 0 & \phi_3(z) & 0 & 0 & \phi_6(z) & 0 & 0 & \cdots \\ 0 & \phi_2(z) & 0 & \phi_4(z) & 0 & 0 & \phi_7(z) & 0 & \cdots \\ 0 & 0 & 0 & 0 & \phi_5(z) & 0 & 0 & \phi_8(z) & \cdots \end{bmatrix} \tag{2}$$

and

$$\{\mathbf{U}(x,y)\} = \{U_1(x,y)U_2(x,y)U_3(x,y)\cdots U_8(x,y)\cdots\}^{\mathrm{T}} \tag{3}$$

Note that $U_1(x,y), U_3(x,y), U_6(x,y), \ldots$ are the in-plane components of displacement terms $u(x,y,z)$. Similarly, $U_2(x,y), U_4(x,y), U_7(x,y), \ldots$ are the in-plane components of displacement terms $v(x,y,z)$. The in-plane components of transverse displacement $w(x,y,z)$ are given by $U_5(x,y), U_8(x,y), \ldots$ The components $U_i(x,y)$ are approximated using triangular elements with order of approximation p_{xy} ($p_{xy} = 2, 3$ in this study). The transverse functions are given in terms of the normalized transverse coordinate $\hat{z} = (2/t)z$ (where t is the thickness of the laminate), with z measured from the middle of the laminate (see Fig. 1).

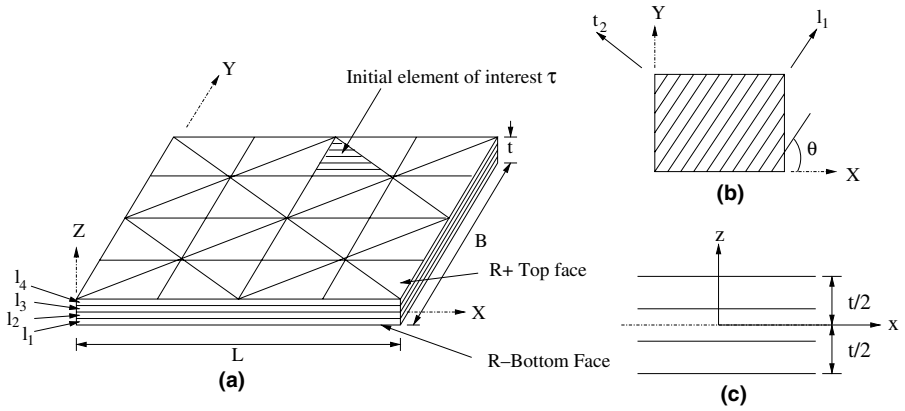

Fig. 1. Plate configuration. (a) Rectangular laminated plate with layers l_i, top and bottom faces R^+ and R^-, respectively, and thickness t, (b) material directions and (c) location of origin of z-axis.

For the higher-order shear deformable model (*HSDT*) the functions $\phi(\hat{z})$ are given as

$$\phi_1(\hat{z}) = \phi_2(\hat{z}) = \phi_5(\hat{z}) = 1, \quad \phi_3(\hat{z}) = \phi_4(\hat{z}) = z,$$
$$\phi_6(\hat{z}) = \phi_7(\hat{z}) = \phi_8(\hat{z}) = \phi_{11}(\hat{z}) = 0,$$
$$\phi_9(\hat{z}) = \phi_{10}(\hat{z}) = z^3, \quad \phi_{11+i}(\hat{z}) = 0, \quad i = 1, 2, \ldots$$

Remark. The HSDT model used here is similar to one proposed by Reddy [11]. The in-plane displacement components have cubic representation and transverse component is constant in laminate thickness. The quadratic term of in-plane displacement components drop out when the zero shear condition on the top and bottom face (i.e. $z = \pm\frac{t}{2}$) of the plate is enforced.

For the hierarchic family of the plate models the transverse functions $\phi(\hat{z})$ are given as

$$\phi_1(\hat{z}) = \phi_2(\hat{z}) = \phi_5(\hat{z}) = 1, \quad \phi_3(\hat{z}) = \phi_4(\hat{z}) = \hat{z},$$
$$\phi_6(\hat{z}) = \frac{h}{2}\{\varphi(\hat{z}) - \varphi(0)\}, \quad \phi_7(\hat{z}) = \frac{h}{2}\{\psi(\hat{z}) - \psi(0)\},$$
$$\phi_8(\hat{z}) = \frac{h}{2}\{\rho(\hat{z}) - \rho(0)\}$$

where

$$\phi(\hat{z}) = \int_{-1}^{\hat{z}} \frac{Q_{44} - Q_{45}}{Q_{44}Q_{55} - Q_{45}^2}\, \mathrm{d}\bar{\hat{z}};$$
$$\psi(\hat{z}) = \int_{-1}^{\hat{z}} \frac{Q_{55} - Q_{45}}{Q_{44}Q_{55} - Q_{45}^2}\, \mathrm{d}\bar{\hat{z}}; \quad \rho(\hat{z}) = \int_{-1}^{\hat{z}} \frac{1}{Q_{33}}\, \mathrm{d}\bar{\hat{z}}$$

where Q_{ij} are the coefficients of the global constitutive relation, in the global xyz-coordinate system. For other transverse functions see [14]. The sequence of models are defined by number of ϕ_is retained in the definition of Eq. (2). This number is denoted as m here. A hierarchic model is then denoted by $HRp_{xy}Mm$. Thus, $HR3M5$ denotes the hierarchic model with $p_{xy} = 3$ and 5-field model. The HSDT model is denoted $HSDTp_{xy}$. E.g. $HSDT3$ denotes HSDT model with $p_{xy} = 3$.

The layerwise model used in this paper is adapted from [22]. The present layerwise plate model is an improvement over the model given in [22], as the original layerwise model had same order transverse representation for all three displacement components, whereas the present layerwise model can have different approximation in transverse direction for individual displacement components. The different approximation for displacement components is used as suggested by Schwab [31], for a single lamina, to take into account the bending and membrane actions. The displacement component u^l, for an element in the lth layer, is given as

$$u^l(x, y, z) = \sum_{j=1}^{n_{xy}} \sum_{k=1}^{p_z^u+1} u_{jk}^l N_j^l(x, y) M_k^l(z) \tag{4}$$

where $n_{xy} = (p_{xy} + 1)(p_{xy} + 2)/2$ for triangular in-plane elements (see Fig. 1); p_{xy} and p_z^u are the in-plane and transverse approximation order (for component u^l) and $N_j(x, y)$ and $M_k(z)$ are in-plane and transverse approximation functions, respectively. Similarly the other components v^l and w^l can be expressed. The in-plane approximation order p_{xy} is the same for u, v and w. The transverse approximation orders for u and v displacement components will be the same, while that for the component w can be different. Hierarchic basis functions will be used for in-plane and transverse representations of the solution components. In this study, $p_{xy} = 2$ or 3 and $p_z^u, p_z^v = 1, 2, 3$ and $p_z^w = 0, 1, 2, 3$ will be used. The layerwise model is denoted by $LMp_{xy}p_z^u p_z^v p_z^w$. E.g. $LM3112$ denotes layerwise model with $p_{xy} = 3$, $p_z^u = 1, p_z^v = 1, p_z^w = 2$.

The solution of the plate problem is decomposed into a membrane and a bending part by Schwab [31]. For the membrane part the in-plane displacement components have symmetric representation, whereas, the transverse displacement has anti-symmetric representation. $(0, 0, 1)$, $(2, 2, 1)$, $(2, 2, 3)$ etc. are the transverse representations of displacement components for membrane part in increasing model order. For the bending part, the in-plane displacement components have anti-symmetric representation, whereas, the transverse displacement has symmetric representation. $(1, 1, 0)$, $(1, 1, 2)$, $(3, 3, 2)$ etc. are the transverse

representations of displacement components for bending part in increasing model order. When the problem is dominated both by membrane and bending actions then the representations of displacements has to be chosen to satisfy both membrane and bending requirements. In this case (1,1,1), (2,2,2), (3,3,3) etc. representations are used. The authors have developed this capability and implemented it successfully in this study.

Remark. The higher-order shear deformation model and hierarchic model do not enforce transverse stress continuity at the interfaces. In the layerwise model the continuity of transverse stress and zero transverse stress on top and bottom faces of laminate can be enforced. Although, in the present layerwise model these conditions are not imposed, it will be shown through numerical examples that the transverse shear stress components show much smaller (it is close to zero in most of the examples studied) jumps than those computed by using higher-order shear deformable and hierarchic models, and the stresses are close to zero on top and bottom faces of the laminate.

3. Finite element formulation

For a given lamina l the constitutive relationship, in the principal material directions is given as

$$\{\bar{\sigma}_{(l)}\} = [C_{(l)}]\{\bar{\epsilon}_{(l)}\} \tag{5}$$

where $\{\bar{\sigma}_{(l)}\} = \{\sigma_{11}^{(l)}\ \sigma_{22}^{(l)}\ \sigma_{33}^{(l)}\ \sigma_{23}^{(l)}\ \sigma_{13}^{(l)}\ \sigma_{12}^{(l)}\}^{\mathrm{T}}$ are the stress components for the layer, and $\{\bar{\epsilon}_{(l)}\} = \{\epsilon_{11}^{(l)}\ \epsilon_{22}^{(l)}\ \epsilon_{33}^{(l)}\ \epsilon_{23}^{(l)}\ \epsilon_{13}^{(l)}\ \epsilon_{12}^{(l)}\}^{\mathrm{T}}$ are the strain components for the layer. Here, 1, 2 and 3 correspond to the three principal material directions (see Fig. 1a). The constitutive relationship in the global xyz-coordinates (for each lamina) can be obtained as

$$\{\sigma_{(l)}\} = [Q_{(l)}]\{\epsilon_{(l)}\} \tag{6}$$

with $\{\sigma_{(l)}\} = \{\sigma_{xx}^{(l)}\ \sigma_{yy}^{(l)}\ \sigma_{zz}^{(l)}\ \sigma_{yz}^{(l)}\ \sigma_{xz}^{(l)}\ \sigma_{xy}^{(l)}\}^{\mathrm{T}}$ and $\{\epsilon_{(l)}\} = \{\epsilon_{xx}^{(l)}\ \epsilon_{yy}^{(l)}\ \epsilon_{zz}^{(l)}\ \epsilon_{yz}^{(l)}\ \epsilon_{xz}^{(l)}\ \epsilon_{xy}^{(l)}\}^{\mathrm{T}}$; $[Q_{(l)}]$ can be obtained from $[C_{(l)}]$ by transformation from the principal material coordinates to global xyz-coordinates. The potential energy, Π, for the structure is given by

$$\Pi = \frac{1}{2}\int_V \{\sigma\}^{\mathrm{T}}\{\epsilon\}\,\mathrm{d}V - \int_{R^+\cup R^-} qw\,\mathrm{d}s \tag{7}$$

where V is the volume enclosed by the plate domain, R^+ and R^- are the top and bottom faces of the plate (see Fig. 1) and $q(x,y)$ is the applied transverse load on these faces.

The solution to the problem, $\mathbf{u}_{\mathrm{ex}}$, is the minimizer of the total potential, Π, and is obtained from the solution of the following weak problem (see [14]):

Find $\mathbf{u}_{\mathrm{ex}} \in H^0(\mathbf{V})$ such that

$$\mathscr{B}(\mathbf{u}_{\mathrm{ex}}, \mathbf{v}) = \mathscr{F}(\mathbf{v}) \quad \forall(\mathbf{v}) \in H^0(\mathbf{V}) \tag{8}$$

where $H^0(\mathbf{V}) = \{\mathbf{U} = [\phi]U | \mathscr{U}(\mathbf{u}) < \infty \text{ and } \mathbf{MU} = \mathbf{0} \text{ on } \Gamma_{\mathrm{D}}\}$. Here, $\Gamma = \Gamma_{\mathrm{N}} \cup \Gamma_{\mathrm{D}}$ is the lateral boundary of the plate with Dirichlet part Γ_{D} and Neumann part Γ_{N}. Note that in this study Dirichlet means the part of lateral boundary where geometric constraints are imposed, while Neumann stands for the stress-free parts of the lateral boundary. Further, $\mathbf{M}$ depends on the type of Dirichlet conditions on the edge, i.e. clamped; soft simple-support; hard simple-support etc.

Hence, we have

$$\mathscr{B}(\mathbf{u}_{\mathrm{ex}}, \mathbf{v}) = \sum_l \mathscr{B}_l(\mathbf{u}_{\mathrm{ex}}, \mathbf{v}) = \sum_l \int_{V_l} \{\sigma_{(l)}(\mathbf{u}_{\mathrm{ex}})\}^{\mathrm{T}}\{\epsilon_{(l)}(\mathbf{v})\}\,\mathrm{d}V_l \tag{9}$$

and

$$\mathscr{F}(\mathbf{V}) = \int_{R^+\cup R^+} qv_3\,\mathrm{d}s \tag{10}$$

where V_l is the volume of the lth lamina in the laminate; v_3 is the transverse component of the test function $\mathbf{v}$.

4. Error estimator for local quantity of interest

In the analysis of laminates for first-ply failure the accurate computation of state of stress at a point is essential. When the finite element analysis is employed, the issue of modeling error (error due to model employed in the analysis of laminate, as compared to three-dimensional elasticity) and discretization error becomes important. Adaptive methods for the control of discretization error are available in the literature (see [32,33]). These are based on control of energy norm of the error, $\|\mathbf{e}\|_{\Omega} = \sqrt{2\mathscr{U}(\mathbf{e})}$ (where $\mathscr{U}(\mathbf{e})$ is the strain energy of the error). This does not guarantee that the quantity of interest is also accurate. In [34] it was shown that the error in the quantity of interest can be given in terms of error in the solution of auxillary problem.

Various smoothening based a posteriori error estimation techniques for laminated composites have been proposed by the authors for the local quantity of interest [35]. Further, estimation and control of the error in the quantity of interest and "one shot" adaptive approach for the control of discretization error was proposed in [36]. In the present study the issue of control of modeling error will not be addressed. In the following sections a summary of error estimation for local quantity of interest and one shot adaptivity are given from [36].

4.1. Definition of error estimator

The variational formulation in (10) is used to obtain the finite element solution $\mathbf{u}_h \in \mathbf{H}_h^0(\mathbf{V})$, where $\mathbf{H}_h^0(\mathbf{V}) = \{\mathbf{u} = [\phi]\mathbf{U};\ U_i \in S_\tau^{p_{xy}},\ i = 1,2,3,\ldots | \mathscr{U}(\mathbf{u}) < \infty,\ \mathbf{MU} = \mathbf{0} \text{ on } \Gamma_{\mathrm{D}}\}$.

Letting $\omega_{2\mathrm{D}}$ be the plate mid surface with boundary $\partial\omega_{2\mathrm{D}}$, we define $S_\tau^{p_{xy}}$ as the set of globally continuous piecewise polynomials of order p_{xy} over each element τ ($\tau \in \omega_{2\mathrm{D}}$):

$$\mathscr{B}(\mathbf{u}_h, \mathbf{v}_h) = \mathscr{F}(\mathbf{v}_h) \quad \forall \mathbf{v}_h \in \mathbf{H}_h^0(\mathbf{V}) \tag{11}$$

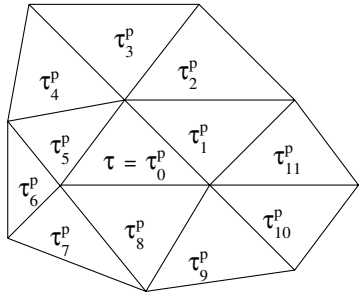

Fig. 2. Element τ with patch P_τ consisting of elements $\{\tau_i^{(p)}\}_{i=0,1,2,\ldots,11}$.

Note that $\mathbf{u}_h = [\phi]\mathbf{U}_h$ is the representation of $\mathbf{u}_h$, following (1). The error in the solution can be given as $\mathbf{e} = \mathbf{u}_{ex} - \mathbf{u}_h$. An approximation to the error can be given as $\mathbf{e}^* = \mathbf{u}^* - \mathbf{u}_h$ where $\mathbf{u}^* \in S_\tau^{p_{xy}+k}$ is obtained for each element τ as described below (see [35] for details). In all the numerical examples $k = 2$ has been employed.

For an element τ let P_τ be the patch of elements in a one-layer neighborhood of τ, as shown in Fig. 2.

Over the patch P_τ, define

$$\mathbf{u}^* = \begin{Bmatrix} u^* \\ v^* \\ w^* \end{Bmatrix} = [\phi]\mathbf{U}^*$$

where

$$U_i^* = \sum_{j=1}^{\mathrm{NDOF}} A_{ij} q_j(x,y)$$

with $\mathrm{NDOF} = (p_{xy}+1+k)(p_{xy}+2+k)/2$; $q_j(x,y)$ as the monomials of order $\leqslant p_{xy}+k$ (see [35] for details) defined in terms of the local coordinates $\hat{x} = x - x_c^\tau$, $\hat{y} = y - y_c^\tau$. Here x_c^τ, y_c^τ are the centroidal coordinates for the element τ.

The coefficients A_{ij} are obtained by minimizing $J = \frac{1}{2}\int_{A_{P_\tau}} |\mathbf{U}^* - \mathbf{U}_h|^2 \,\mathrm{d}A$ where A_{P_τ} is the area of the patch P_τ (where $A_{P_\tau} \subset \omega_{2D}$). This definition is called the L_2 projection based error estimator (see [35] for details).

4.2. Auxillary problem

Let us consider the domain of Fig. 1. Let us further assume that we are interested in the value of stress component σ_{xx} in the topmost layer, for all points in the element τ (shown shaded in Fig. 1a).

In order to accurately obtain the point-wise information in τ, we will let $\sigma_{xx,\mathrm{avg}}^{(l)} = \frac{1}{v_\tau^l}\int_{v_\tau^l} \sigma_{xx}\,\mathrm{d}v$ as the quantity of interest. Here $V_\tau^l = A_\tau t_l$ is the volume enclosed by the element τ in the lth layer. Hence,

$$\sigma_{xx,\mathrm{avg}}^{(l)} = \frac{1}{A_\tau t_l}\int_{z=z_{l-1}}^{z_l}\int_{A_\tau} (\sigma_{xx}\,\mathrm{d}A)\,\mathrm{d}z \tag{12}$$

with t_l as the thickness of the lth layer; z_{l-1} and z_l as the lower and upper z coordinate for the lth layer; A_τ is the area of element τ (or group of elements).

Remark. In this study, the quantity of interest used is the stress component which contributes maximum to the failure index for the Tsai–Wu criterion.

Corresponding to $\sigma_{xx,\mathrm{avg}}^{(l)}$ we define the following auxillary problem:

Find $\mathbf{G} \in \mathbf{H}^0(\mathbf{V})$ such that

$$\mathscr{B}(\mathbf{G},\mathbf{v}) = \sigma_{xx,\mathrm{avg}}^{(l)}(\mathbf{v}) = \mathscr{F}(\mathbf{v}) \quad \forall \mathbf{v} \in \mathbf{H}^0(\mathbf{V}) \tag{13}$$

Letting $\mathbf{G}_h \in \mathbf{H}_h^0(\mathbf{V})$ be the finite element solution for $\mathbf{G}$, we have

$$\mathscr{B}(\mathbf{G}_h,\mathbf{v}_h) = \sigma_{xx,\mathrm{avg}}^{(l)}(\mathbf{v}_h) = \mathscr{F}(\mathbf{v}_h) \quad \forall \mathbf{v}_h \in \mathbf{H}_h^0(\mathbf{V}) \tag{14}$$

Note that $\mathbf{u}_h$ and $\mathbf{G}_h$ can be solved for simultaneously (see [36] for details). Multiple regions can be handled simultaneously.

4.3. Estimators for error in quantity of interest

From the previous section we have

$$\mathscr{B}(\mathbf{G},\mathbf{u}_{ex}-\mathbf{u}_h) = \mathscr{F}(\mathbf{u}_{ex}) - \mathscr{F}(\mathbf{u}_h) = \mathscr{F}(\mathbf{u}_{ex}-\mathbf{u}_h) = \mathscr{F}(\mathbf{e}) \tag{15}$$

From the orthogonality property of the error in the finite element solution, we have

$$|\mathscr{B}(\mathbf{G}-\mathbf{G}_h,\mathbf{u}_{ex}-\mathbf{u}_h)| = |\mathscr{F}(\mathbf{e})| \tag{16}$$

which implies (see [36])

$$|\mathscr{F}(\mathbf{e})| \leqslant \|\mathbf{e}_\mathbf{u}\|\|\mathbf{e}_\mathbf{G}\| \tag{17}$$

where $\mathbf{e}_\mathbf{u} = \mathbf{e}$ stands for the error in the actual solution and $\mathbf{e}_\mathbf{G}$ stands for the error in the auxillary problem.

4.4. Definition of a posteriori error estimators for local quantity of interest

Replacing $\mathbf{e}_\mathbf{u}$ with the estimate $\mathbf{e}_\mathbf{u}^*$ and $\mathbf{e}_\mathbf{G}$ with the estimate $\mathbf{e}_\mathbf{G}^*$, we can get many definitions of the estimators (see [36]), for the error in the quantity of interest. Here we employ

Estimator (E):

$$|\mathscr{F}(\mathbf{e})|_E = \sum_\tau |\mathscr{B}(\mathbf{e}_\mathbf{u}^*,\mathbf{e}_\mathbf{G}^*)| \tag{18}$$

4.5. One-shot adaptivity for quantity of interest

We let $\mathbf{u}_h^{(p_{xy})}$, $\mathbf{G}_h^{(p_{xy})}$ be the finite element solutions of the order p_{xy} for $\mathbf{u}_{ex}$ and $\mathbf{G}$. Thus, we can approximate error $\mathbf{e}_\mathbf{u}$ as $\mathbf{e}_\mathbf{u} \approx \mathbf{e}_\mathbf{u}^{(p_{xy}+1)} = \mathbf{u}_h^{(p_{xy}+1)} - \mathbf{u}_h^{(p_{xy})}$ and hence $\mathscr{F}(\mathbf{e}) \approx \mathscr{F}(\mathbf{e}_\mathbf{u}^{(p_{xy}+1)})$. It can be shown that $\mathscr{F}(\mathbf{e}_\mathbf{u}^{(p_{xy}+1)}) = \sum_\tau \mathscr{B}(\mathbf{e}_\mathbf{G}^{(p_{xy}+1)},\mathbf{e}_\mathbf{u}^{(p_{xy}+1)})$.

Letting τ be the element of interest and P, the one-layer neighborhood of τ, the total error can be partitioned into two parts as follows:

$$|\mathscr{F}(\mathbf{e})| \leqslant |\mathscr{F}_1(\mathbf{e})| + |\mathscr{F}_2(\mathbf{e})|$$

where

$$\mathscr{F}_1(\mathbf{e}) = \sum_{\tau\in P} \mathscr{B}(\mathbf{e_u}, \mathbf{e_G}), \quad \mathscr{F}_2(\mathbf{e}) = \sum_{\tau\in P'} \mathscr{B}(\mathbf{e_u}, \mathbf{e_G}) \tag{19}$$

where P' is the set of elements lying outside P. Following [27], $\mathscr{F}_1(\mathbf{e})$ is the local part of the error and $\mathscr{F}_2(\mathbf{e})$ is the "pollution" in the quantity of interest (i.e. far-field influence).

The goal of the adaptive process is to refine the given mesh selectively such that the total error is below the specified tolerance, i.e.

$$|\mathscr{F}(\mathbf{e})| \leqslant \eta |\mathscr{F}(\mathbf{u}_h)| \tag{20}$$

where $\mathscr{F}(\mathbf{u}_h)$ is the computed value of the desired quantity of interest; $|\mathscr{F}(\mathbf{e})| = |\mathscr{F}(\mathbf{e})|_E$ is obtained using definition E for the error. Following [33], we will define $r_\tau = \frac{h_d}{h}$ as the ratio of the desired (h_d) to the actual mesh size (h) of the element τ. The desired mesh size is obtained by minimizing

$$\sum_\tau \frac{1}{r_\tau^2}$$

subject to constraint (20). Thus, we define the new objective function (to be minimized) as

$$J = \sum_\tau \frac{1}{r_\tau^2} + \lambda_1 \left(\sum_{\tau\in P} \chi_{d,\tau}^2 - \mathscr{F}_{d,1} \right) + \lambda_2 \left(\sum_{\tau\in P'} \chi_{d,\tau}^2 - \mathscr{F}_{d,2} \right) \tag{21}$$

where $\chi_{d,\tau} = |\mathscr{B}(\hat{\mathbf{e}}_\mathbf{u}, \hat{\mathbf{e}}_\mathbf{G})|$ is the desired contribution to the total error from element τ; $\hat{\mathbf{e}}_\mathbf{u}, \hat{\mathbf{e}}_\mathbf{G}$ are the desired errors in the element τ; λ_1 and λ_2 are Lagrange multipliers; $\mathscr{F}_{d,1} = \eta_1 |\mathscr{F}(\mathbf{u}_h)|$ and $\mathscr{F}_{d,2} = \eta_2 |\mathscr{F}(\mathbf{u}_h)|$ are the desired errors in the region P and P', respectively (here $\eta = \eta_1 + \eta_2$).

Minimizing J with respect to r_τ, λ_1 and λ_2 we get

$$r_\tau = \frac{\mathscr{F}_{d,1}^{1/p_{xy}}}{\left(\sum_{\tau\in P} \chi_{a,\tau}^{4/(p_{xy}+2)}\right)^{1/p_{xy}} \cdot \chi_{a,\tau}^{2/(p_{xy}+2)}}, \quad \tau \in P \tag{22}$$

$$r_\tau = \frac{\mathscr{F}_{d,2}^{1/2p_{xy}}}{\left(\sum_{\tau\in P'} \chi_{a,\tau}^{2/(p_{xy}+1)}\right)^{1/2p_{xy}} \cdot \chi_{a,\tau}^{1/(p_{xy}+1)}}, \quad \tau \in P' \tag{23}$$

Using the computed values of r_τ, the desired mesh sizes can be computed. The mesh can be locally refined several times based on the desired mesh size.

Remark. In this study $\eta_1 = \eta_2 = 5\%$ is taken.

5. Tsai–Wu failure criterion

It is a complete polynomial criterion and is an extension of the criterion used for anisotropic materials (see [41]).

The Tsai–Wu criterion is given by

$$FI_{TW} = F_i\sigma_i + F_{ij}\sigma_i\sigma_j \geqslant 1 \tag{24}$$

where F_i and F_{ij} are the strength tensor terms and σ_i are the stress components and

$$\begin{aligned}
&F_1 = \frac{1}{X_T} - \frac{1}{X_C}; \quad F_2 = \frac{1}{Y_T} - \frac{1}{Y_C}; \quad F_3 = \frac{1}{Z_T} - \frac{1}{Z_C};\\
&F_{11} = \frac{1}{X_T X_C}; \quad F_{22} = \frac{1}{Y_T Y_C}; \quad F_{33} = \frac{1}{Z_T Z_C};\\
&F_{44} = \frac{1}{R^2}; \quad F_{55} = \frac{1}{S^2}; \quad F_{66} = \frac{1}{T^2};\\
&F_{12} = -\frac{1}{2}\frac{1}{\sqrt{X_T X_C Y_T Y_C}}; \quad F_{13} = -\frac{1}{2}\frac{1}{\sqrt{X_T X_C Z_T Z_C}};\\
&F_{23} = -\frac{1}{2}\frac{1}{\sqrt{Y_T Y_C Z_T Z_C}}
\end{aligned} \tag{25}$$

where X, Y and Z are the strengths in 1, 2 and 3 directions, respectively. Subscript T denotes tensile strength, and C denotes compressive strength. R, S and T are shear strengths in 23, 13 and 12 planes, respectively.

6. Numerical results

One of the major goals of this paper is to do a critical analysis of various families of plate models, with respect to the quality of the point-wise stresses obtained using the models. The effect of in-plane approximation order, model order and type will also be investigated here. Numerical experiments are conducted with the plate models to compare the transverse deflection and stress profiles for numerous ply orientations, stacking sequences and boundary conditions under transverse loadings. Here symmetric and antisymmetric laminates are considered. Three types of transverse loadings are considered, namely, uniform pressure, sinusoidal and cylindrical bending. The results are compared with available exact solutions for these problems (see [37–40]).

The numerical results are arranged in two sections. In the first section, the effect of the plate models on the accuracy of point-wise data, i.e. transverse deflection and all the stress components at a point, is addressed. The stress components are either computed directly using the constitutive equations of (6), or the equilibrium equations are used to obtain the transverse normal and shear stresses.

From the equilibrium equations, the component σ_{xz} at any z location from bottom face of the laminate is computed as

$$\sigma_{xz|_z} = -\int_{z=\frac{-t}{2}}^{z} (\sigma_{xx,x} + \tau_{xy,y})\, dz \tag{26}$$

For the right-hand side quantities the constitutive equations are used. Similar procedure for the components τ_{yz} and σ_{zz} is used. In order to extract σ_{zz}, the $\tau_{xz,x}$ and $\tau_{yz,y}$ are computed directly from the finite element solution, using the constitutive equations.

In the second section, the effect of the models and discretisation on the accuracy of first-ply failure load is addressed.

6.1. Effect of model on accuracy of point-wise data

In this section, the problems considered in [37–40] are taken. These problems are posed over rectangular domains, and exact solutions are given in [37–40]. The exact solutions have no singularities and weak boundary layer (if it exists). Hence, the asymptotics, in the finite element solution, is obtained with relatively crude uniform meshes. These problems become good benchmark to test for accuracy of plate models.

6.1.1. Comparison of transverse deflections

The goal of this numerical experiment is to compare the value of transverse displacement components obtained using various models, and in-plane discretisation, with the exact three-dimensional elasticity results reported in [37,38], for [0/90/0] laminate sequence with material properties as given in Table 1. The plate has dimension a along x-axis and b along y-axis, and is subjected to transverse sinusoidal loading of the form:

$$q(x,y) = q_0(x,y)\sin\left(\frac{\pi x}{a}\right)\sin\left(\frac{\pi y}{b}\right)$$

All edges of the plate are simply supported (see Table 2 for all BCs used). The transverse deflection at $(\frac{a}{2},\frac{b}{2},0)$ is reported in Tables 3 and 4. The mesh used for these computations is shown in Fig. 3.

In this study the following cases have been studied:

Case 1: Rectangular plate with dimensions $b = 3a$ with all the lamina of equal thickness. The transverse deflection is normalized as $\bar{w} = \frac{100E_{22}w}{q_0 S^4 t}$ where $S = \frac{a}{t}$, $\bar{z} = \frac{z}{t}$. The models used are *HSDT*2, *HR*2*M*11 and *LM*2332. The transverse deflection for this case is given in Table 3.

Case 2: Square plate with cross-ply laminae, such that outer laminae with orientation 0° are of equal thickness and total thickness of 0° layers is equal to total thickness of 90° laminae. The transverse deflection is normalized as $w^* = \frac{\pi^4 Q w}{12 q_0 S^4 t}$, where $Q = 4G_{12} + [E_{11} + E_{22}(1 + 2\nu_{23})]/(1 - \nu_{12}\nu_{21})$. Here *HSDT*3, *HR*3*M*11 and *LM*3332 models are used. The transverse deflections for this case are given in Table 4. Numbers in parenthesis show the % error with respect to exact solution.

Table 1
Material properties for graphite/epoxy [37–40]

Property	E_{11}	E_{22}	G_{12}	G_{23}	$\nu_{12} = \nu_{23}$
Values	25×10^6 psi	10^6 psi	0.5×10^6 psi	0.2×10^6 psi	0.25

Table 2
Boundary conditions

Boundary	Along $x = 0, a$	Along $y = 0, b$
Clamped (C)	$u = v = w = 0$	$u = v = w = 0$
Hard simple supported (S)	$v = w = 0$	$u = w = 0$
Free (F)	$u, v, w \neq 0$	$u, v, w \neq 0$

Table 3
Comparison of transverse displacement ($\bar{w}$) for [0/90/0], rectangular laminate ($b = 3a$) under sinusoidal loading, SSSS

S	Exact [37]	*LM*2332	*HSDT*2	*HR*2*M*11
2	8.170	8.16 (0.12)	8.044 (1.54)	8.027 (1.75)
4	2.820	2.820 (0.00)	2.644 (6.24)	2.705 (4.07)
10	0.919	0.918 (0.11)	0.866 (5.76)	0.897 (2.39)
20	0.610	0.609 (0.16)	0.593 (2.78)	0.602 (1.31)
50	0.520	0.520 (0.00)	0.516 (0.76)	0.517 (0.57)
100	0.508	0.507 (0.19)	0.504 (0.78)	0.505 (0.59)

Table 4
Comparison of transverse deflection (w^*); square [0/90/0] laminate under sinusoidal loading, SSSS

S	Exact [38]	*LM*3332	*HSDT*3	*HR*3*M*11
2	11.767	11.770 (−0.03)	12.137 (−3.14)	10.949 (6.95)
4	4.491	4.491 (0.00)	4.382 (2.43)	4.318 (3.85)
10	1.709	1.709 (0.00)	1.165 (5.50)	1.682 (2.70)
20	1.189	1.189 (0.00)	1.164 (2.50)	1.182 (0.70)
50	1.031	1.031 (0.00)	1.017 (1.35)	1.028 (0.29)
100	1.008	1.008 (0.00)	0.995 (1.26)	1.006 (0.19)

Middle layer has twice the thickness of each of the outer layer.

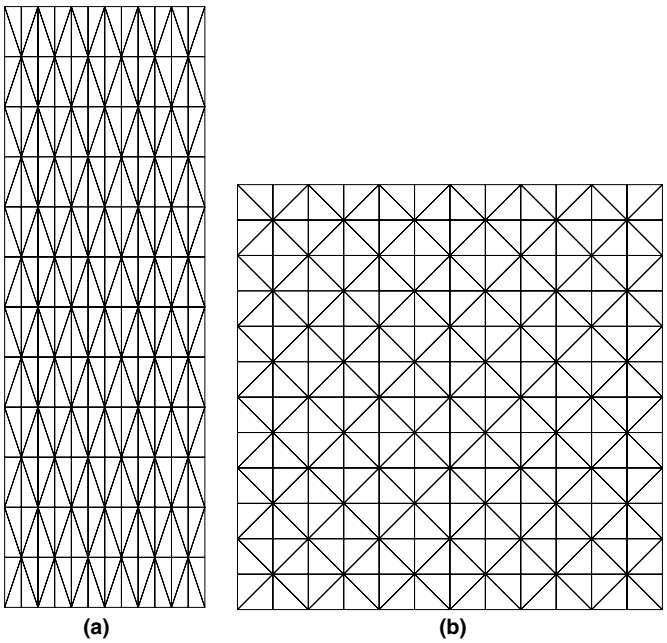

Fig. 3. Uniform meshes used for computing the transverse deflections. (a) Mesh for rectangular laminate and (b) mesh for square laminate.

From these tables we observe that

1. The *LM*2332 and *LM*3332 models predicts the transverse deflection accurately for all the aspect ratios. The error in the values ranges from 0% to 0.2%.
2. The *HSDT*2, *HSDT*3 and *HR*2*M*11, *HR*3*M*11 models are far from the exact one for the aspect ratios up to $S = 10$. The error for this aspect ratios ranges from 1.5% to 7%.

3. For the *HSDT*2, *HSDT*3 and *HR*2*M*11, *HR*3*M*11 models with aspect ratios $S > 10$ the displacement is close to exact. The error is 0.1–4%. The hierarchic models are closer to the exact one, as compared to the HSDT models.

Case 3: Problem considered is same as in case 1, except that $b = a$ and model used is *LM*3332. The variation of normalised in-plane displacement, $\bar{u} = \frac{E_{22}u(0,\frac{b}{2},\bar{z})}{q_0 t S^3}$, is shown in Fig. 4. From this figure it can be seen that the displacement is anti-symmetric and as S increases the transverse variation of the displacement tends to a straight line. For small S, the effect of transverse shear is prominent and this leads to nonlinear warping of the normal (see [40]). From this result it is obvious that the HSDT and hierarchic models will capture the displacement field better for thin plates. For moderately thick to thick plates, the conventional higher-order shear deformable theories will not be able to compute the piecewise behavior of u (or v), as these models use smooth transverse representation of u, v and w.

6.1.2. Comparison of stresses

Here, various stress components for symmetric and anti-symmetric laminates, under cylindrical bending, are compared with the exact values (for three-dimensional analysis) given in [39,40]. For the analysis, all cases use *HSDT*2, *HR*2*M*5, *HR*2*M*8, *HR*2*M*11 and *LM*2332 models.

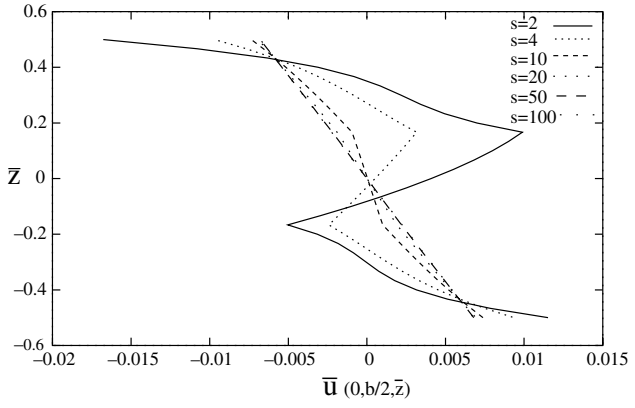

Fig. 4. Variation of in-plane displacement for [0/90/0], square laminate under sinusoidal loading, all edges simple supported, $p_{xy} = 3$.

Case 1: In this case [0/90/0] laminate is considered. All the laminae are of equal thickness. The cylindrical loading is of the form $q(x,y) = q_0 \sin(\frac{\pi x}{a})$. The laminate is infinite along y-axis and simply supported along the edges $x = 0$, a. The normalized stress components

$$(\bar{\sigma}_{xx}, \bar{\sigma}_{zz}, \bar{\tau}_{xz}) = \frac{1}{q_0}\left(\sigma_{xx}\left(\frac{a}{2},\bar{z}\right), \sigma_{zz}\left(\frac{a}{2},\bar{z}\right), \tau_{xz}(0,\bar{z})\right)$$

obtained directly from the finite element solution are shown in Figs. 5 and 6 for $S = 4$. The stress components obtained using the equilibrium approach of post-processing are shown in Fig. 7.

Case 2: In this case, [165/−165] laminate under cylindrical loading, as in case 1 above, is considered. All the laminae are of equal thickness. The normalized stress components $\bar{\sigma}_{xx} = \frac{1}{q_0 S^2}\sigma_{xx}(\frac{a}{2},\bar{z})$ and $\bar{\tau}_{xz} = \frac{1}{q_0 S}\tau_{xz}(0,\bar{z})$ are shown for $S = 10$ in Figs. 8 and 9.

Case 3: The problem description is same as given in case 1 of previous subsection. The exact point-wise values of the stress components at various points and for different S are available from [37]. These are compared with the values obtained using the *LM*2332 model in Table 5. The reported normalised stress components are

$$(\bar{\sigma}_{xx}, \bar{\sigma}_{yy}, \bar{\tau}_{xy}) = \frac{1}{q_0 S^2}\left(\sigma_{xx}\left(\frac{a}{2},\frac{b}{2},\bar{z}\right), \sigma_{yy}\left(\frac{a}{2},\frac{b}{2},\bar{z}\right), \tau_{xy}(0,0,\bar{z})\right)$$

and

$$(\bar{\tau}_{xz}, \bar{\tau}_{yz}) = \frac{1}{q_0 S}\left(\tau_{xz}\left(0,\frac{b}{2},\bar{z}\right), \tau_{yz}\left(\frac{a}{2},0,\bar{z}\right)\right)$$

Remark. In Tables 5 and 7, for the transverse shear stresses ($\bar{\tau}_{xz}$ and $\bar{\tau}_{yz}$) for given S, the first row gives the value at $\bar{z} = 0$. In the second row the maximum values and in the third row their location quoted in parenthesis, is reported.

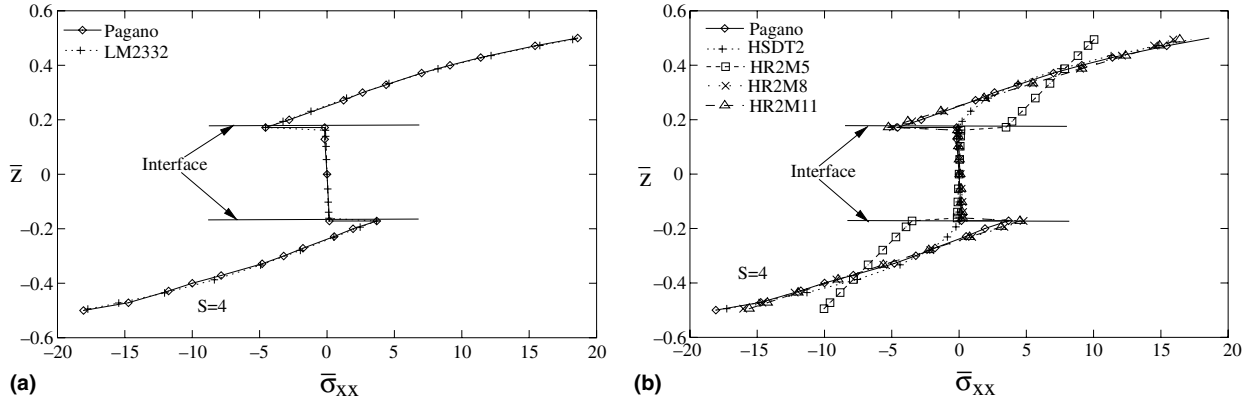

Fig. 5. Comparison of in-plane stresses distribution for [0/90/0] laminate under cylindrical bending, FSFS, $p_{xy} = 2$. (a) In-plane normal stress (*LM*2332, $S = 4$) and (b) in-plane normal stress (*HSDT*2 and *HR*2*M*5, *HR*2*M*8 and *HR*2*M*11, $S = 4$).

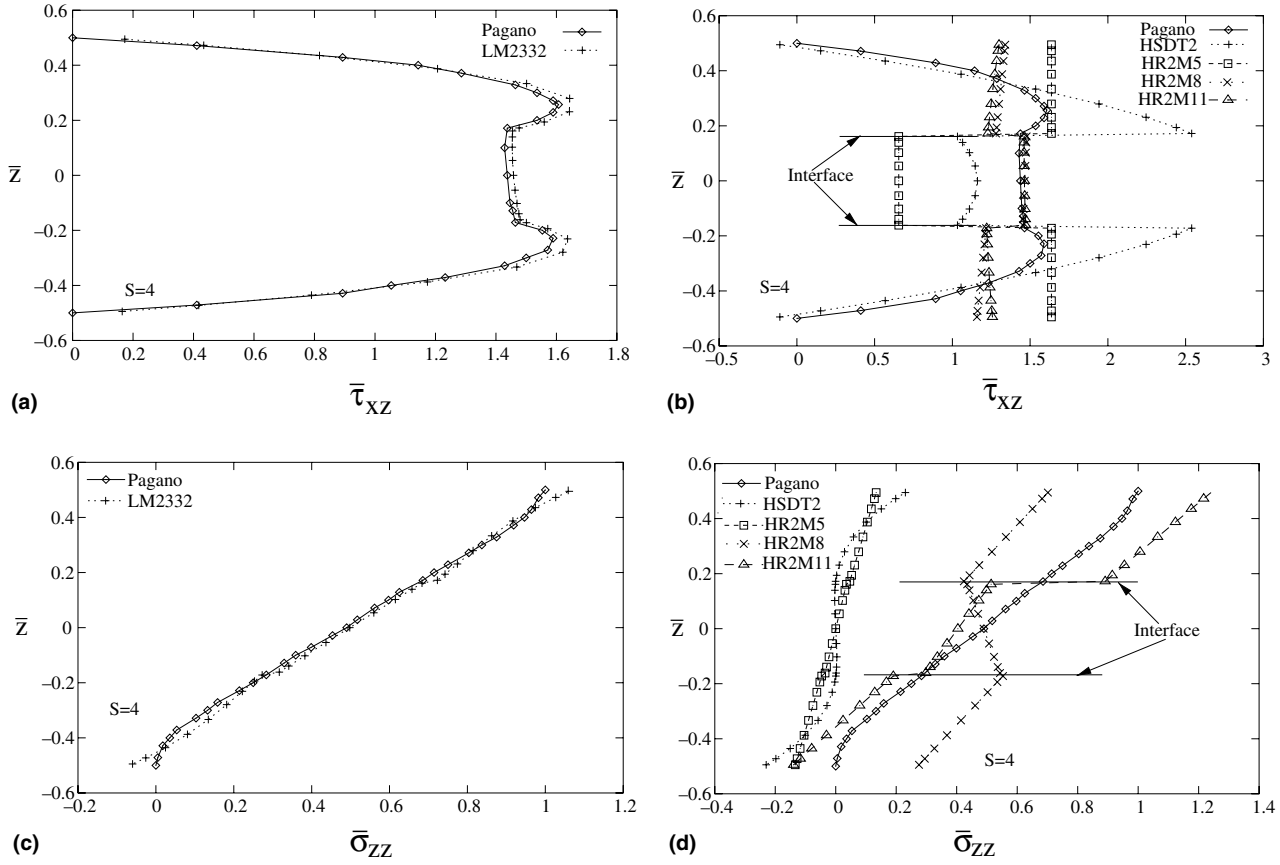

Fig. 6. Comparison of transverse stresses distribution for [0/90/0] laminate under cylindrical bending, FSFS $p_{xy} = 2$. (a) Transverse shear stress ($LM2332$, $S = 4$), (b) transverse shear stress ($HSDT2$ and $HR2M5$, $HR2M8$ and $HR2M11$, $S = 4$), (c) transverse normal stress ($LM2332$, $S = 4$) and (d) transverse normal stress ($HSDT2$ and $HR2M5$, $HR2M8$ and $HR2M11$, $S = 4$).

From the results it is observed that

1. The in-plane stress components are accurately predicted by all higher-order models.
2. The transverse shear stress components computed directly from finite element solution is accurate for the $LM2332$ model whereas, those obtained by $HSDT2$ and $HR2M5$, $HR2M8$ and $HR2M11$ models are significantly different both qualitatively and quantitatively.
3. Using the equilibrium approach of post-processing leads to more accurate transverse stress components for all the models.
4. The $LM2332$ model predicts accurately the point-wise values of the stress components for all the values of S.

Case 4: The problem description is same as in case 1 of previous subsection. The plate is square and sandwiched with face sheets of material as given in Table 1 and thickness of each face sheet as $\frac{t}{10}$. The core material is transversely isotropic in z-direction and the material properties are as given in Table 6. The point-wise values of the stress components for various S, obtained with $LM2332$ model are reported in Table 7. Normalisation of stresses is same as in case 3.

From this table it is observed that

1. The $LM2332$ model predicts all the stress components accurately.
2. The stress component σ_{xx} has sharp gradient in the face sheets (see [37] for more details). Even this feature has been captured accurately by the layerwise model.

6.2. Effect of models on accuracy of predicted failure load

Following [42] the laminates considered are $[0/90]_S$ and $[-45/45/-45/45]$. The plate is either clamped on all edges or hard simple supported. The top face of the plate is subjected to uniform transverse load $q(x,y) = q_0$. The plate dimensions are $a = 228.9$ mm (9 in.), $b = 127$ mm (5 in.). The material properties and lamina thickness used in these computations are given in Table 8. The first ply failure load is nondimensionalised as

$$\mathrm{FLD} = \frac{q_0}{E_{22}} S^4$$

In computing the local state of stress, the equilibrium based post-processing is used to get the transverse stresses.

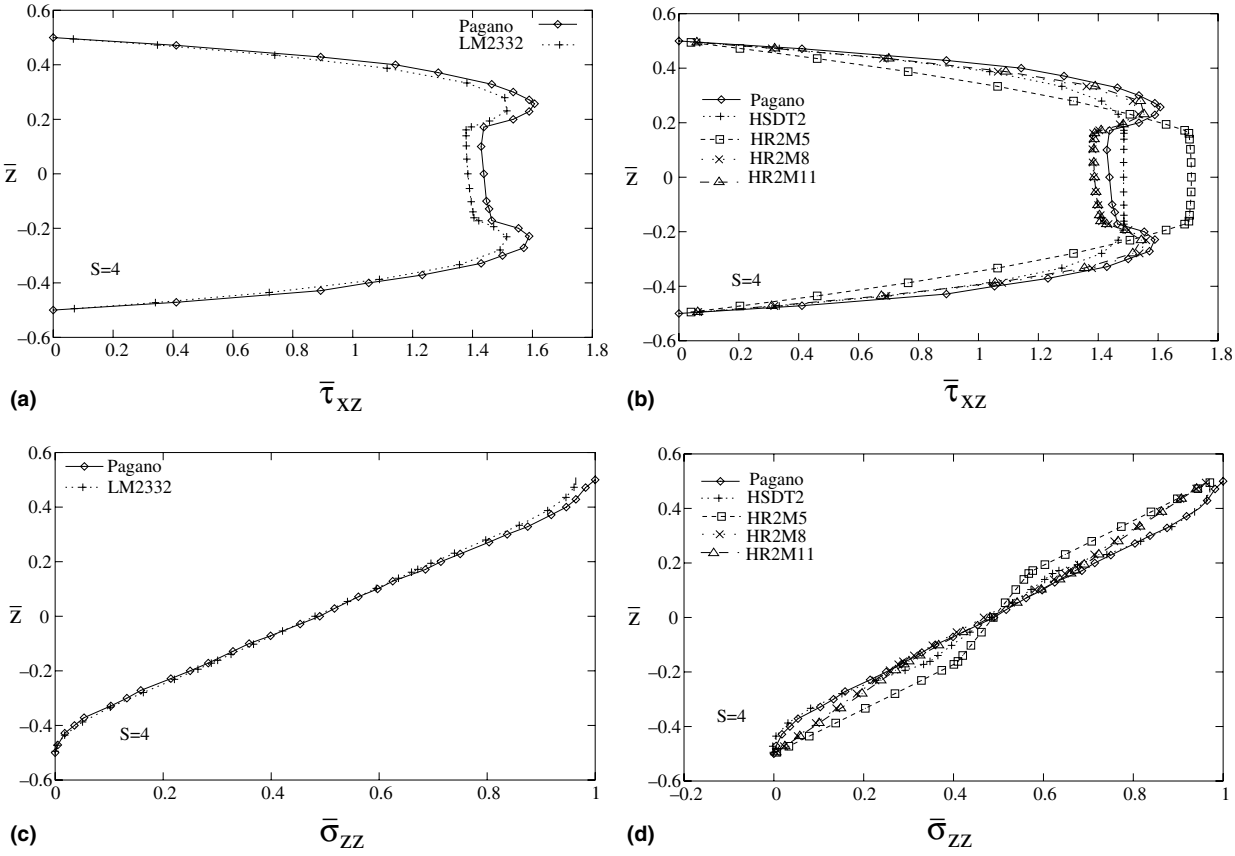

Fig. 7. Comparison of transverse stresses distribution for [0/90/0] laminate under cylindrical bending, FSFS $p_{xy} = 2$ (equilibrium approach). (a) Transverse shear stress ($LM2332$, $S = 4$), (b) transverse shear stress ($HSDT2$ and $HR2M5$, $HR2M8$ and $HR2M11$, $S = 4$), (c) transverse normal stress ($LM2332$, $S = 4$) and (d) transverse normal stress ($HSDT2$ and $HR2M5$, $HR2M8$ and $HR2M11$, $S = 4$).

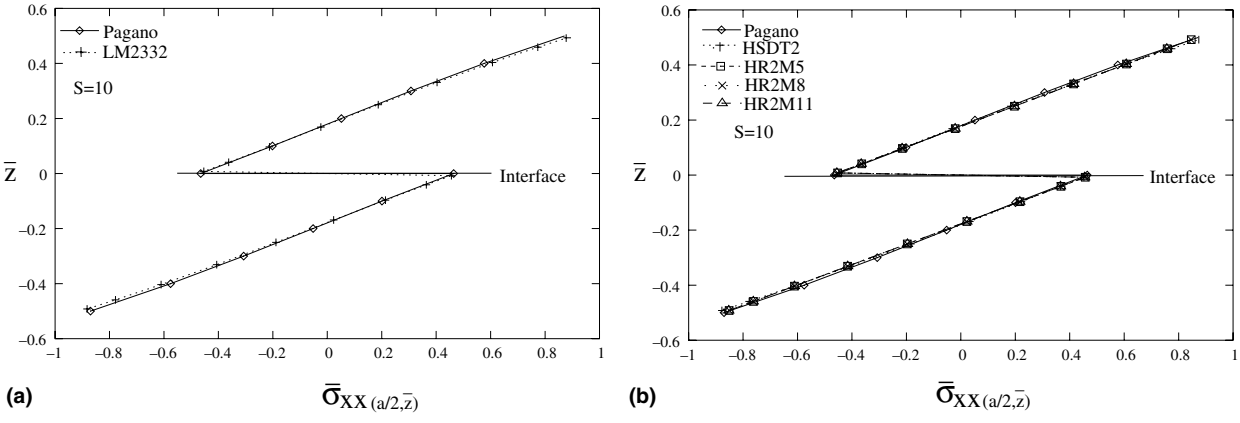

Fig. 8. Comparison of in-plane normal and shear stress distribution for [165/−165] laminate under cylindrical bending, $S = 10$, FSFS, $p_{xy} = 2$. (a) $LM2332$ model and (b) $HSDT2$ and $HR2M5$, $HR2M8$ and $HR2M11$ models.

The results obtained from the present analysis using $HSDT2$, $HR2M5$, $HR2M8$, $HR2M11$ and $LM2332$ are compared with those reported in [42].

The computed failure load depends on the accuracy of the lamina level stress. In general, there is no a priori information about the quality of the local stress. Hence, an adaptive approach with the capability to estimate discretisation error in the local stresses and refine mesh accordingly to bring the error down to acceptable tolerance, is desired. For the fixed model, the focussed adaptive approach is employed to recompute the failure load. Here, the stress component contributing maximum to the

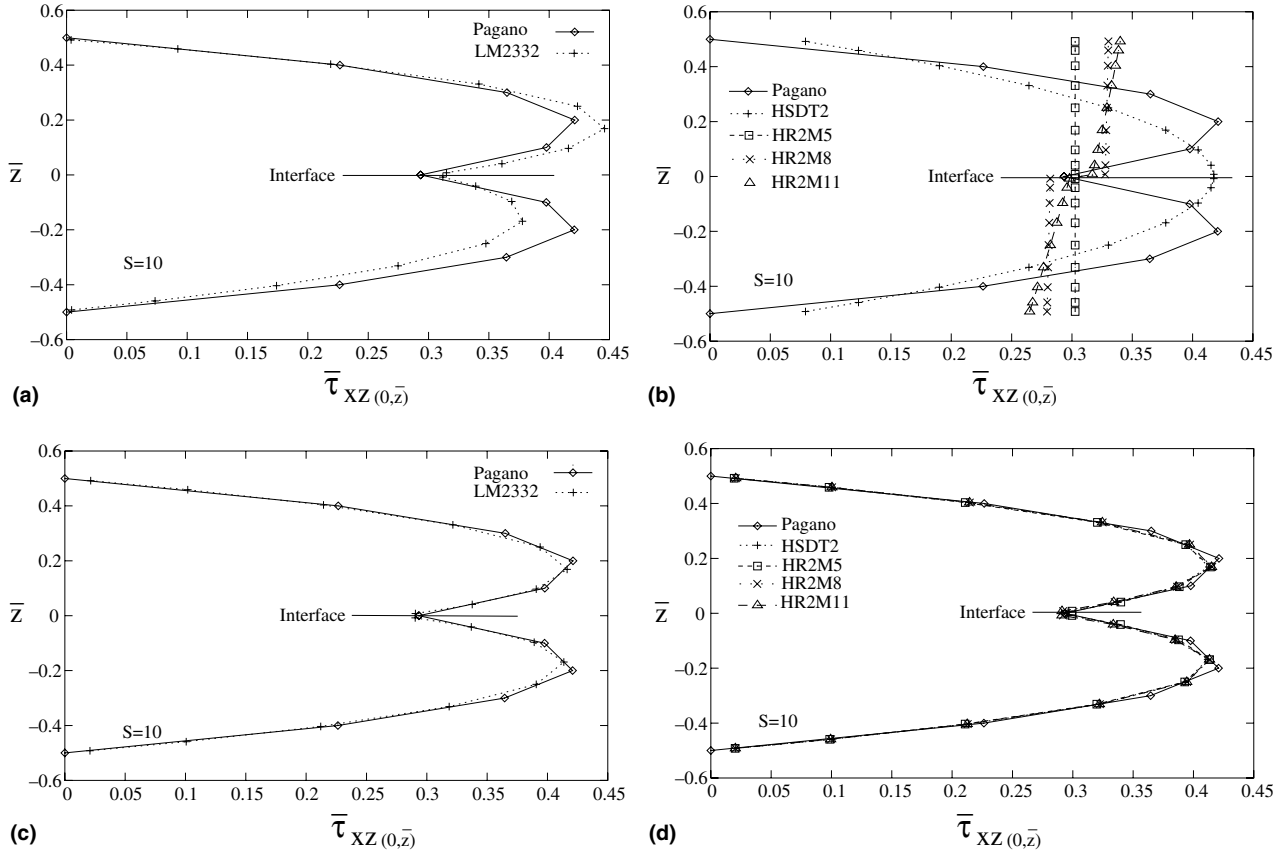

Fig. 9. Comparison of transverse shear stress distribution (τ_{xz}) for [165/−165] laminate under cylindrical bending, $S = 10$, FSFS, $p_{xy} = 2$. (a) $LM2332$ model with direct stress, (b) $HSDT2$ and $HR2M5$, $HR2M8$ and $HR2M11$ models with direct stress, (c) $LM2332$ model with equilibrium approach and (d) $HSDT2$ and $HR2M5$, $HR2M8$ and $HR2M11$ models with equilibrium approach.

Table 5
Comparison of stresses for three-layered, rectangular ($b = 3a$), cross-ply laminate, SSSS

S	$\bar{\sigma}_{xx}(\frac{a}{2},\frac{a}{2},\pm 0.5)$		$\bar{\sigma}_{yy}(\frac{a}{2},\frac{a}{2},\pm\frac{1}{6})$[a]		$\bar{\tau}_{xz}(0,\frac{b}{2},0)$		$\bar{\tau}_{yz}(\frac{a}{2},0,0)$		$\bar{\tau}_{xy}(0,0,\pm 0.5)$	
	Exact	$LM3332$	Exact	$LM3332$	Exact	$LM3332$	Exact	$LM3332$	Exact	$LM3332$
2	2.13	2.13	0.230	0.229	0.257	0.257	0.0668	0.0671	−0.0564	−0.0564
	−1.62	−1.62	−0.268	−0.267	0.455	0.466	0.0673	0.0673	0.0548	0.0548
					(0.3)	(0.3)	(−0.03)	(0.03)		
4	1.14	1.14	0.109	0.109	0.351	0.351	0.0334	0.0338	−0.0269	−0.0269
	−1.10	−1.10	−0.119	−0.119	0.387	0.390			0.0281	0.0281
					(0.27)	(0.27)				
10	0.726	0.727	0.0418	0.0418	0.420	0.420	0.0152	0.0161	−0.0120	−0.0120
	−0.725	−0.727	−0.0435	−0.0435	0.420	0.420			0.0123	0.0123
					(−0.03)	(−0.03)				
20	0.650	0.652	0.0294	0.0295	0.434	0.435	0.0119	0.0139	−0.0093	−0.0093
	−0.650	−0.652	−0.0299	−0.0300					0.0093	0.0093
50	0.628	0.631	0.0259	0.0259	0.439	0.445	0.0110	0.0158	−0.0084	−0.0085
	−0.628	−0.631	−0.0259	−0.0260					0.0084	0.0085
100	0.624	0.632	0.0253	0.0253	0.439	0.462	0.0108	0.0195	−0.0083	−0.0084
	−0.624	−0.632	−0.0253	−0.0253					0.0083	0.0084

[a] The maximum values indicated for $\bar{\sigma}_{yy}$ occur in the central layer.

Table 6
Material properties for sandwich plate [37]

Property	$E_{xx} = E_{yy}$	E_{zz}	$G_{xz} = G_{yz}$	G_{zz}	$v_{xz} = v_{yz} = v_{xy}$
Values	0.04×10^6 psi	0.5×10^6 psi	0.06×10^6 psi	0.016×10^6 psi	0.25

Table 7
Comparison of stresses for three-layered, square, sandwich plate, SSSS

S	$\bar{\sigma}_{xx}\left(\frac{a}{2},\frac{a}{2},\pm\frac{1}{2}\right)$		$\bar{\sigma}_{xx}\left(\frac{a}{2},\frac{a}{2},\pm\frac{1}{2.5}\right)$		$\bar{\sigma}_{yy}\left(\frac{a}{2},\frac{a}{2},\pm\frac{1}{2}\right)$		$\bar{\tau}_{xz}\left(0,\frac{b}{2},0\right)$		$\bar{\tau}_{yz}\left(\frac{a}{2},0,0\right)$		$\bar{\tau}_{xy}\left(0,0,\pm\frac{1}{2}\right)$	
	Exact	*LM*3332	Exact	*LM*3332	Exact	*LM*3332	Exact	*LM*3332	Exact	*LM*3332	Exact	*LM*3332
2	3.278	3.234	−2.220	−2.174	0.4517	0.4506	0.185	0.185	0.1399	0.1403	−0.2403	−0.2385
	−2.653	−2.693	1.668	1.705	−0.3919	−0.3956	0.320	0.318	0.1402	0.1404	0.2338	0.2358
							(0.44)	(0.44)	(−0.08)	(0.08)		
4	1.556	1.556	−0.233	−0.233	0.2595	0.2596	0.239	0.239	0.1072	0.1078	−0.1437	−0.1437
	−1.512	−1.517	0.196	0.202	−0.2533	−0.2536					0.1481	0.1483
10	1.153	1.154	0.628	0.626	0.1104	0.1105	0.300	0.299	0.0527	0.0535	−0.0707	−0.0708
	−1.152	−1.142	−0.629	−0.626	−0.1099	−0.1100					0.0717	0.0718
20	1.110	1.112	0.810	0.808	0.0700	0.0702	0.317	0.317	0.0361	0.0376	−0.0511	−0.0511
	−1.110	−1.112	−0.810	−0.808	−0.0700	−0.0701					0.0511	0.0514
50	1.099	1.103	0.867	0.866	0.0569	0.0573	0.323	0.326	0.0306	0.0358	−0.0446	−0.0449
	−1.099	−1.103	−0.867	−0.866	−0.0569	−0.0573					0.0446	0.0449
100	1.098	1.106	0.875	0.879	0.0550	0.0556	0.324	0.337	0.0297	0.0422	−0.0437	−0.0442
	−1.098	−1.106	−0.875	−0.879	−0.0550	−0.0556					0.0437	0.0442

Table 8
Material properties for T300/5208 graphite/epoxy (Pre-preg) [42]

Property	Value
E_{11}	132.5 GPa
$E_{22}=E_{33}$	10.8 GPa
$G_{12}=G_{13}$	5.7 GPa
G_{23}	3.4 GPa
$v_{12}=v_{13}$	0.24
v_{23}	0.49
X_T	1515 MPa
X_C	1697 MPa
$Y_T=Z_T=Y_C=Z_C$	43.8 MPa
R	67.6 MPa
$S=T$	86.9 MPa
Ply thickness, t_i	0.127 mm

Tsai–Wu first-ply failure criterion is used as the quantity of interest. In Tables 9–12 the first-ply failure loads are given. In these tables

1. The superscript *a* shows all the values of failure loads and corresponding failure index obtained using mesh shown in Fig. 10a.
2. The superscript *b* shows the value of the failure index obtained with the same load as in *a* and the adapted mesh (e.g. see Fig. 10b).
3. The superscript *c* shows the first-ply failure load for the adapted mesh. The initial mesh and final adapted mesh for HSDT and hierarchic models for a representative problem are shown in Fig. 10.

Note that the first-ply failure load for layerwise model is computed using only the initial mesh.

From the results we observe that:

1. For the initial mesh, the failure loads predicted by all the models are lower than those obtained by [42] (rows with superscript *a*).

Table 9
First-ply failure loads; all edges clamped, $[0/90]_S$ laminate under uniform transverse loading, $p_{xy}=2$

Model	FLD	Coordinates		Layer	Location	FI_{TW}	Max. σ
		x	y				
Ref. [42]	19,050.9	≈5.00	≈65.00	1	Bottom	–	
HSDT2^a	17,172.8	107.51	0.563	4	Top	1.00	σ_{22}
HSDT2^b	17,172.8	112.71	0.14	4	Top	1.85	
HSDT2^c	12,612.9	112.71	0.14	4	Top	1.00	
HR2M5^a	17,180.3	107.51	0.56	4	Top	1.00	σ_{22}
HR2M5^b	17,180.3	112.71	0.14	4	Top	1.85	
HR2M5^c	12,612.7	112.71	0.14	4	Top	1.00	
HR2M8^a	17,175.3	107.51	0.56	4	Top	1.00	σ_{22}
HR2M8^b	17,175.3	112.71	0.14	4	Top	1.85	
HR2M8^c	12,612.0	112.71	0.14	4	Top	1.00	
HR2M11^a	16,531.3	107.51	0.56	4	Top	1.00	σ_{22}
HR2M11^b	16,531.3	112.71	0.14	4	Top	1.80	
HR2M11^c	12,322.5	112.71	0.14	4	Top	1.00	
LM2332^a	17,123.6	107.51	0.56	4	Top	1.00	σ_{22}

Table 10
First-ply failure loads; all edges clamped, [−45/45/−45/45] laminate under uniform transverse loading, $p_{xy}=2$

Model	FLD	Coordinates		Layer	Location	FI_{TW}	Max. σ
		x	y				
Ref. [42]	39,354.8	≈115.00	≈125.00	1	Bottom	–	
HSDT2^a	31,463.7	107.51	0.56	4	Top	1.00	σ_{22}
HSDT2^b	31,463.7	112.71	0.14	4	Top	1.82	
HSDT2^c	23,377.6	112.71	0.14	4	Top	1.00	
HR2M5^a	31,486.1	107.51	0.56	4	Top	1.00	σ_{22}
HR2M5^b	31,486.1	112.71	0.14	4	Top	1.82	
HR2M5^c	23,383.7	112.71	0.14	4	Top	1.00	
HR2M8^a	31,403.1	107.51	0.56	4	Top	1.00	σ_{22}
HR2M8^b	31,403.1	112.71	0.14	4	Top	1.82	
HR2M8^c	23,350.7	112.71	0.14	4	Top	1.00	
HR2M11^a	31,672.2	121.38	126.43	4	Top	1.00	σ_{22}
HR2M11^b	31,672.2	116.18	126.85	4	Top	1.75	
HR2M11^c	23,955.1	116.18	126.85	4	Top	1.00	
LM2332^a	32,549.2	107.51	0.56	1	Bottom	1.00	σ_{22}

Table 11
First-ply failure loads; all edges simple supported, $[0/90]_S$ laminate under uniform transverse loading, $p_{xy} = 2$

Model	FLD	Coordinates		Layer	Location	FI_{TW}	Max. σ
		x	y				
Ref. [42]	11,646.5	≈5.00	≈5.00	4	Top	–	
$HSDT2^a$	9948.9	115.46	46.18	4	Top	1.00	σ_{22}
$HSDT2^b$	9948.9	117.91	62.67	4	Top	1.07	
$HSDT2^c$	9620.2	117.91	62.67	4	Top	1.00	
$HR2M5^a$	9951.1	119.20	50.27	4	Top	1.00	
$HR2M5^b$	9951.1	117.91	62.67	4	Top	1.07	σ_{22}
$HR2M5^c$	9623.1	117.91	62.67	4	Top	1.00	
$HR2M8^a$	9949.1	115.46	46.18	4	Top	1.00	σ_{22}
$HR2M8^b$	9949.1	117.91	62.67	4	Top	1.07	
$HR2M8^c$	9620.5	117.91	62.67	4	Top	1.00	
$HR2M11^a$	10,055.6	115.65	43.66	4	Top	1.00	σ_{22}
$HR2M11^b$	10,055.6	117.91	62.67	4	Top	1.05	
$HR2M11^c$	9786.7	117.91	62.67	4	Top	1.00	
$LM2332^a$	11,954.4	115.65	43.66	1	Bottom	1.00	σ_{22}

Table 12
First-ply failure loads; all edges simple supported, $[-45/45/-45/45]$ laminate under uniform transverse loading, $p_{xy} = 2$

Model	FLD	Coordinates		Layer	Location	FI_{TW}	Max. σ
		x	y				
Ref. [42]	32,513.5	≈115	≈65	4	Top	–	
$HSDT2^a$	25,802.4	138.28	66.13	4	Top	1.00	σ_{22}
$HSDT2^b$	25,802.4	136.99	73.26	4	Top	1.08	
$HSDT2^c$	24,729.1	136.99	73.26	4	Top	1.00	
$HR2M5^a$	25,807.7	90.62	60.86	4	Top	1.00	σ_{22}
$HR2M5^b$	25,807.7	91.91	53.73	4	Top	1.09	
$HR2M5^c$	24,729.5	91.91	53.73	4	Top	1.00	
$HR2M8^a$	25,687.1	90.62	60.86	4	Top	1.00	σ_{22}
$HR2M8^b$	25,687.1	91.91	53.73	4	Top	1.08	
$HR2M8^c$	24,727.7	91.91	53.73	4	Top	1.00	
$HR2M11^a$	30,791.5	31.22	0.56	1	Bottom	1.00	
$HR2M11^b$	30,791.5	0.25	0.96	4	Top	1.39	σ_{22}
$HR2M11^c$	26,173.7	0.25	0.96	4	Top	1.00	
$LM2332^a$	31,078.2	1.20	107.16	4	Top	1.00	σ_{22}

2. The locations predicted by all the models are either close to one obtained by [42] or are corresponding symmetric points.
3. Failure loads predicted by the $HSDT2$ and $HR2M5$, $HR2M8$, and $HR2M11$ models are close while those predicted by $LM2332$ are slightly higher than these.
4. For the failure load obtained using uniform mesh, the failure index computed using the adapted mesh is 88% more. This is due to the increased flexibility of the numerical solution for the adapted mesh.
5. With the adapted mesh the error in the failure load computations can be close to 40%.
6. The failure locations for the $HSDT2$ model and $HR2M5$, $HR2M8$, and $HR2M11$ models are in the same region before and after the use of discretization error control (see Fig. 11).

It is obvious that a suitably refined mesh, along with proper post-processed values of the transverse stresses, is necessary to obtain reliable values of the first-ply failure load.

6.2.1. A study of the reasons for change in calculated failure loads

The failure loads obtained in this study are, in general, significantly lower than those reported in the literature. In all the cases considered, failure initiates at a point near a boundary edge. It is well-known that (see [25–30]) the solution near the boundary, for thin domains, is affected by the following factors:

1. *Boundary layer effect:* Due to the imposed boundary constraints and material characteristics, the exact solution to these problems may display a strong boundary-layer effect. The boundary layer can be represented as (see [29]) $u_i(x,y) = \chi_i(x,y)e^{-\alpha\rho/t}$ where $\alpha > 0$, t is thickness of laminate, ρ is distance from edge.
2. *Regularity of solution:* For certain boundary constraints, the parameter t effects the regularity of the solution for certain models (see [27]).
3. *Effect of corner singularities:* Due to reentrant corners in the domain, the solution has a $r^{\alpha}(\log r)^{\beta}$ type representation in the vicinity of the corner (r is scaled distance from corner, which may depend on $1/t$).
4. *Effect of locking:* For $t \to 0$, the finite element solution converges at a suboptimal rate. Using higher p_{xy} and suitably higher model (e.g. $HR2M8$) leads to relatively "locking free" approximation.
5. *Discretisation error:* As low order elements are used ($p_{xy} = 2$ or 3), discretisation error can be significant.
6. *Choice of representation of failure index:* The polynomial representation of failure index makes it sensitive to changes in values of certain stress components.

In order to demonstrate the boundary-layer effect, let us take the $[30/-30/30]$ square laminated plate with $a = 38.1$ mm, $S = 10,\ 100$; with material properties of Table 8. Uniformly distributed transverse load of intensity $q_0 = 0.01$ MPa is applied. For this plate, we plot the variation of $\bar{u}(x,\frac{b}{2},0) = u(x,\frac{b}{2},0)E_{22}/(tS^3)$ and $\bar{w}(x,\frac{b}{2},0) = w(x,\frac{b}{2},0)E_{22}/(tS^3)$ for $HR3M8$ and $LM3112$ and $LM3332$ approximations, when the plate is clamped on all edges. The problem is solved using a uniform and geometrically graded mesh, as shown in Fig. 12. Note that following [29], only one layer of graded refinement with mesh size $O(p_{xy}t)$ is required, but here several graded layers are taken as an "overkill". From Fig. 13, it can be observed that

1. The boundary layer in $\bar{u}(x,y,z)$ is sharp for $S = 100$ (thin plate) and has a sharp gradient at a point close to the boundary.
2. All models capture the location of the peak point, but show different intensities (values) at this point. For lower models, the boundary layer may be less pronounced as compared to the exact three-dimensional one.

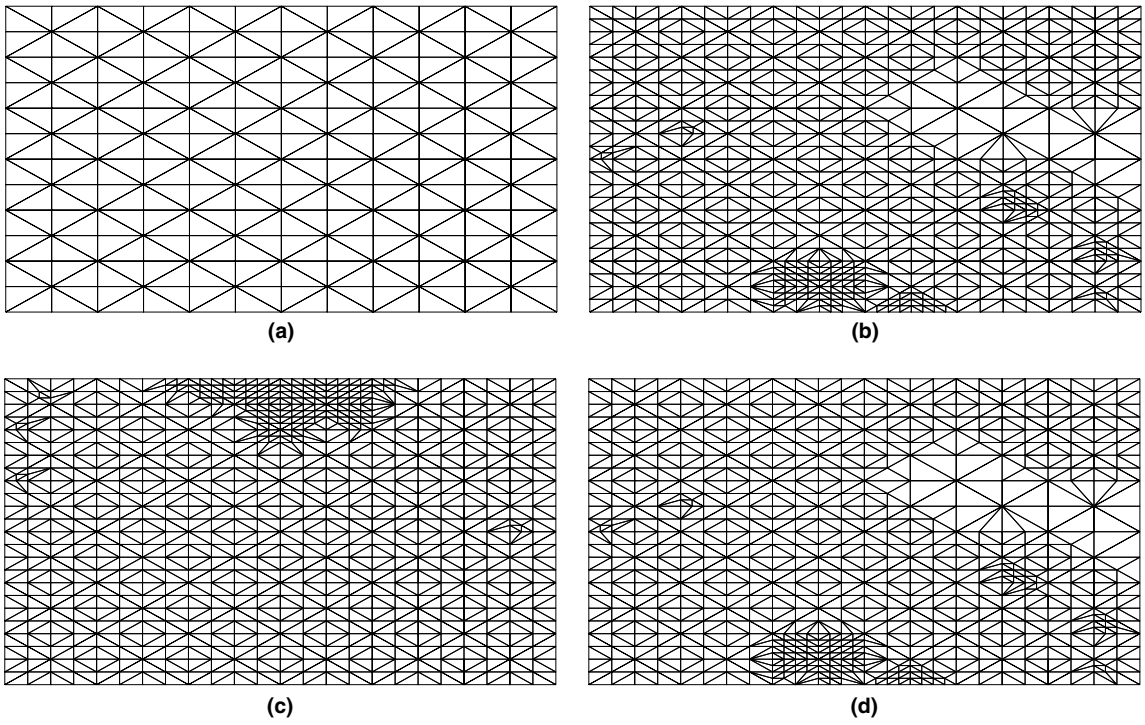

Fig. 10. Adapted mesh for all edges clamped $[-45/45/-45/45]_S$ laminate under uniform load, all edges clamped $p_{xy} = 2$. (a) Initial mesh, (b) $HR2M5$ model, (c) $HR2M11$ model and (d) $HSDT2$ model.

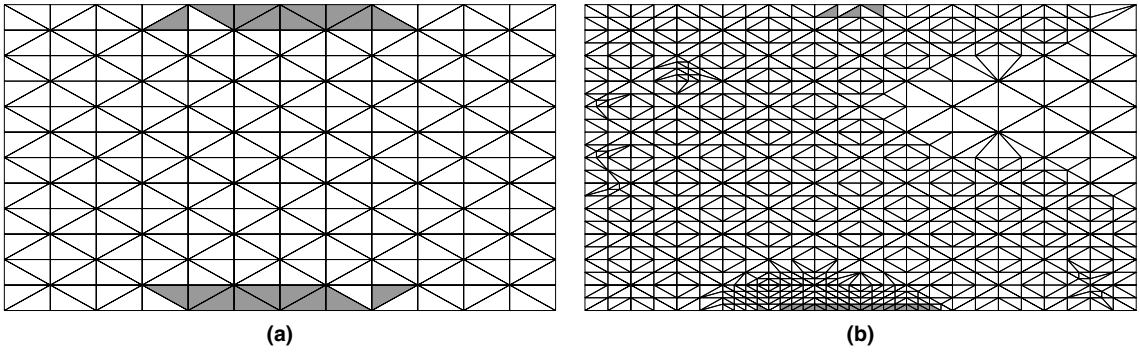

Fig. 11. Region of failure for $[-45/45/-45/45]$ laminate, all edges clamped. (a) Failure region with initial mesh and (b) failure region with adapted mesh.

3. The uniform mesh completely misses the sharp boundary layer and hence gives a different displacement profile everywhere.
4. $\bar{w}(x, y, z)$ does not have any boundary layer effect, while $\bar{v}(x, y, z)$ behaves similar to $\bar{u}(x, y, z)$ and hence $\bar{v}(x, \frac{b}{2}, 0)$ is not plotted here.
5. For thicker plates ($S = 10$) the boundary layer is less pronounced.

From the observations, it is clear that with uniform meshes, the boundary layer in the solution (if it exists) will not be captured (for thin domains), hence leading to significantly different representation of stress at the boundary. Further, a suitably higher model should be used at the boundary to capture the boundary layer profile.

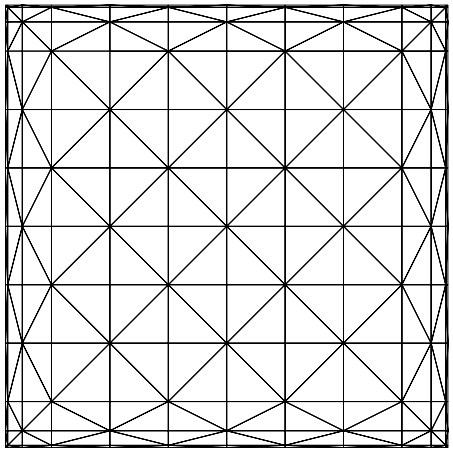

Fig. 12. Graded mesh for boundary layer computation.

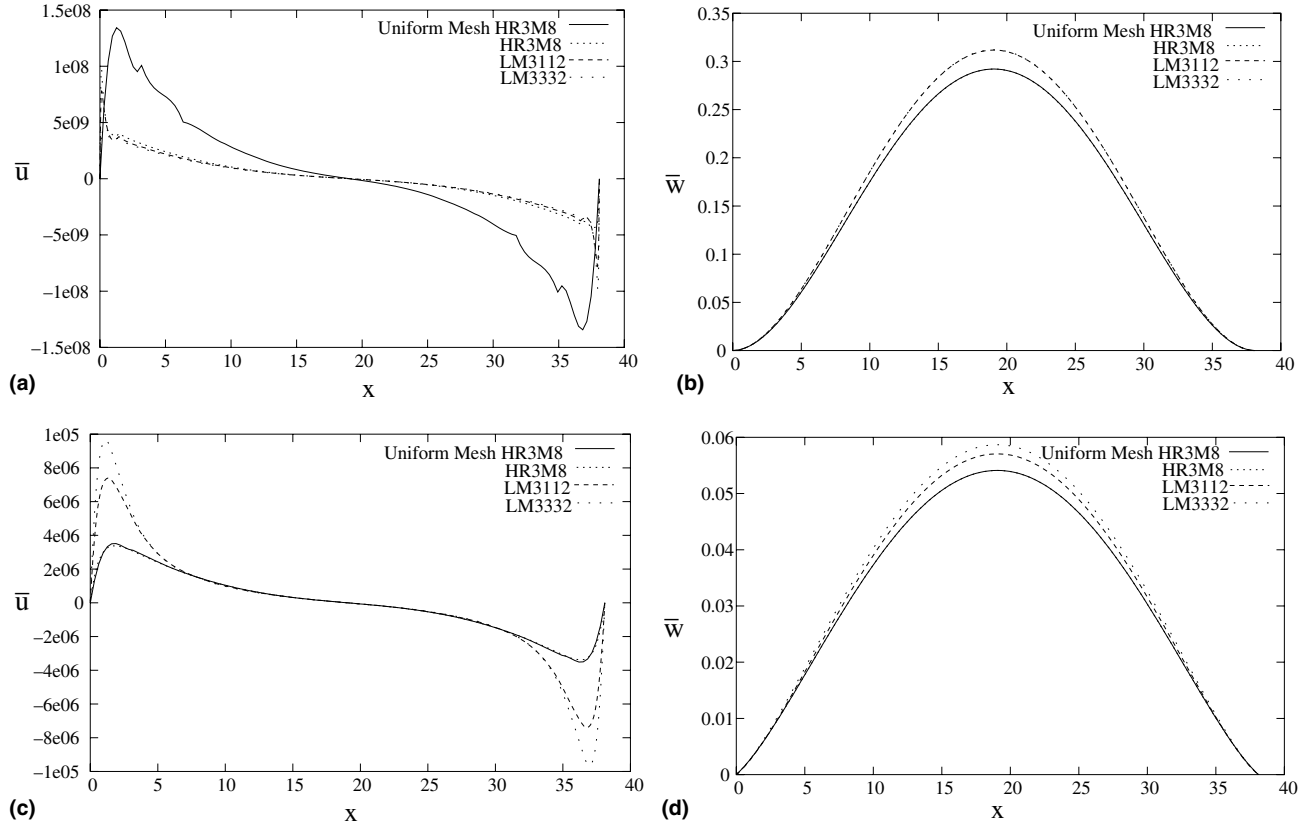

Fig. 13. Displacement variation for [30/−30/30] laminate, all edges clamped. (a) $S = 100$, (b) $S = 100$, (c) $S = 10$ and (d) $S = 10$.

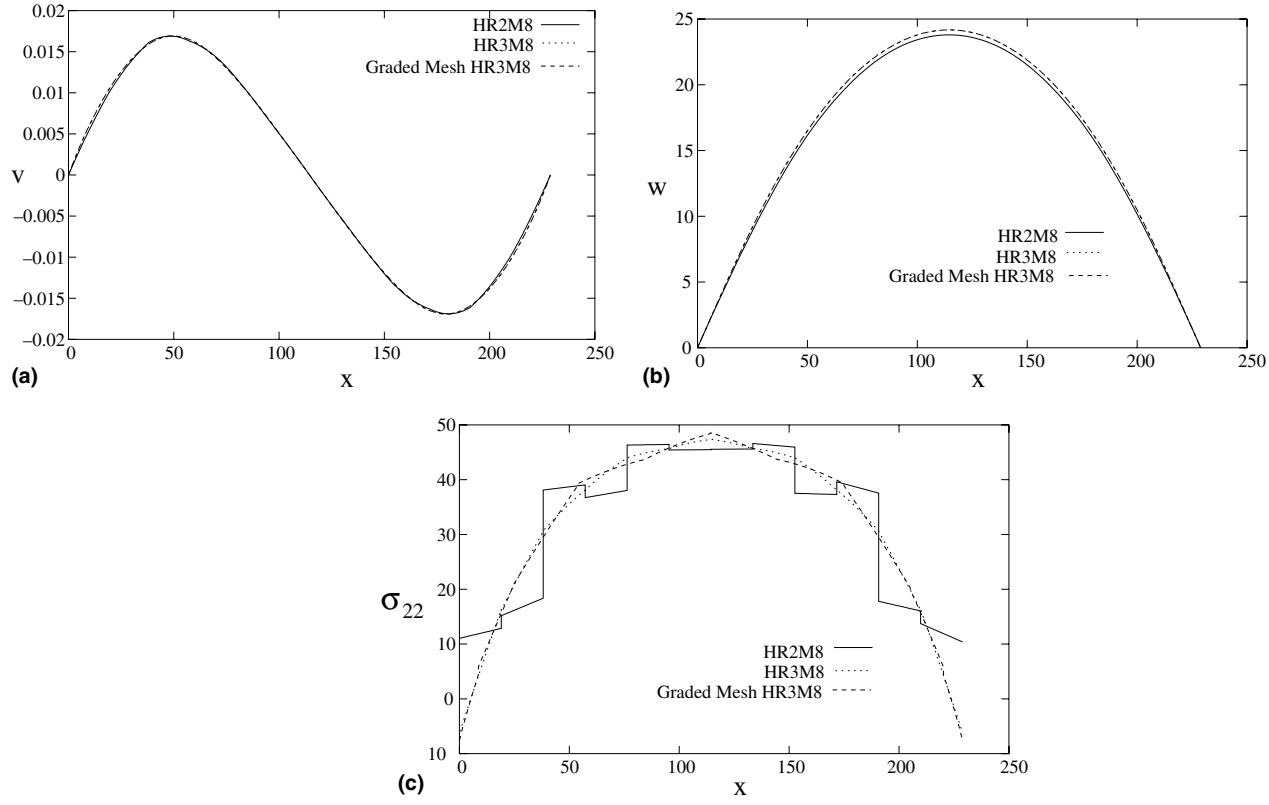

Fig. 14. Displacement and stress variation for [−45/45/−45/45] laminate, all edges simple supported. (a) v displacement variation, (b) w displacement variation and (c) σ_{22} variation.

Let us also take the [−45/45/−45/45] laminate, simply supported on all edges. $S = 450$ is taken (as given in previous section), and load corresponds to failure load obtained earlier. The problem is solved using $HR2M8$ and $HR3M8$. In this case $u(x, \frac{b}{2}, 0)$ is zero, hence displays no boundary layer effects. $v(x, \frac{b}{2}, 0)$ varies as shown in Fig. 14a. The plot of $w(x, \frac{b}{2}, 0)$ is given in Fig. 14b. In Fig. 14c $\sigma_{22}(x, \frac{b}{2}, \frac{t}{2})$ (on top face of plate) is plotted. From the figures it can be seen that

1. In this case, boundary layer does not play a role.
2. Predominantly, the quality of the solution depends on some effects of locking (as seen by the changes in w and σ_{22}) and mostly on discretisation error.
3. For low order elements, i.e. $p_{xy} = 2$ or 3, as is popularly used, the coarse mesh solution may be "stiffer" (especially at the boundary) resulting in higher predicted failure load.

As shown in [36], the a posteriori error estimator overestimates actual error when the boundary layer is not resolved and when locking exists. This leads to over refinement of the mesh in the desired region, and thus a significant improvement of the numerical solution. This is apparent from the local stress values reported in Tables 13 and 15. The focussed adaptivity is based on control of error in a region and hence leads to suitable refinement of the mesh in the regions contributing significantly to the local error. This is the reason why the adaptive meshes used in this study give significantly lower failure loads.

It should be noted that the effect of the regularity of the solution will also be resolved by the adapted mesh.

In order to study the effect of adaptivity on the location of failure point and the value of failure load, we carried out a detailed study for [−45/45/−45/45] clamped laminate for the $HSDT2$ model with equilibrium stresses. In the study the following terms are used:

1. *Initial load:* the load for the first-ply failure with initial mesh.
2. *Final load:* the load for the first-ply failure with adapted mesh.
3. *Initial point:* the point (in xy-plane) for the first-ply failure with initial mesh and initial load.
4. *Final point:* the point (in xy-plane) for the first-ply failure with adapted mesh and final load.

The stress values at these two failure points for the initial mesh and final adapted mesh with initial load and final load applied, and the term-wise contribution to the failure index is given in Tables 13–16.

From the results it is observed that

1. The component which contributes maximum to the failure index in all cases is σ_{22}.
2. In all the cases the largest component among all the stress components is σ_{11}, but its contribution to the failure index is small (as compared to σ_{22}) as strength in fibre direction is the highest.

Table 13
Stress values at failure points for $HSDT2$ with initial load, CCCC

Quantity	Unadapted mesh		Adapted mesh	
	Initial point	Final point	Initial point	Final point
σ_{11}	−226.90527	−228.78367	−282.84943	−300.01144
σ_{22}	−43.53871	−43.80961	−55.05408	−57.88164
σ_{33}	2.86241	1.45395	1.21977	4.92509
τ_{23}	0.00524	0.00155	0.02052	0.00030
τ_{13}	0.00753	0.00236	0.08155	0.02122
τ_{12}	−23.01129	−23.17125	−28.98974	−30.55400

Table 14
Contribution to failure index for $HSDT2$ with initial load, CCCC

Contribution due to term	Unadapted mesh		Adapted mesh	
	Initial point	Final point	Initial point	Final point
F_1	−0.01606	−0.01619	−0.02090	−0.02124
F_2	0.00000	0.00000	0.00000	0.00000
F_3	0.00000	0.00000	0.00000	0.00000
F_{11}	0.02003	0.02035	0.03391	0.03501
F_{22}	0.98811	1.00044	1.68029	1.74636
F_{33}	0.00427	0.00111	0.00081	0.01264
F_{44}	0.00000	0.00000	0.00000	0.00000
F_{55}	0.00000	0.00000	0.00000	0.00000
F_{66}	0.07012	0.07109	0.11913	0.12362
F_{12}	−0.14066	−0.14272	−0.23868	−0.24726
F_{13}	0.00925	0.00474	0.00523	0.02104
F_{23}	0.06496	0.03321	0.03682	0.14859
Index	1.00000	0.97203	1.61661	1.81879

Table 15
Stress values at failure points for $HSDT2$ with final load, CCCC

Quantity	Unadapted mesh		Adapted mesh	
	Initial point	Final point	Initial point	Final point
σ_{11}	−168.59107	−169.98673	−219.36488	−222.90911
σ_{22}	−32.34935	−32.55064	−42.18489	−43.00617
σ_{33}	2.12678	1.08028	0.92427	3.65935
τ_{23}	0.00390	0.00115	0.00215	0.00022
τ_{13}	0.00560	0.00176	0.01141	0.01577
τ_{12}	−17.09743	−17.21628	−22.28501	−22.70168

Table 16
Contribution to failure index for $HSDT2$ with final load, CCCC

Contribution due to term	Unadapted mesh		Adapted mesh	
	Initial point	Final point	Initial point	Final point
F_1	−0.01193	−0.01203	−0.01553	−0.01577
F_2	0.00000	0.00000	0.00000	0.00000
F_3	0.00000	0.00000	0.00000	0.00000
F_{11}	0.01105	0.01124	0.01872	0.01933
F_{22}	0.54548	0.55229	0.92761	0.96408
F_{33}	0.00235	0.00061	0.00044	0.00698
F_{44}	0.00000	0.00000	0.00000	0.00000
F_{55}	0.00000	0.00000	0.00000	0.00000
F_{66}	0.03871	0.03925	0.06576	0.06824
F_{12}	−0.07765	−0.07878	−0.13176	−0.13650
F_{13}	0.00511	0.00262	0.00288	0.01162
F_{23}	0.03586	0.01833	0.02033	0.08202
Index	0.54898	0.53353	0.88845	1.00000

3. For the adapted mesh, the in-plane stress values increase significantly (up to 40%) when compared to the stresses obtained for the initial mesh.
4. For the adapted mesh, the critical value of σ_{22} is obtained for a smaller load.
5. The contribution of the transverse stress components is small.
6. The cross-terms, e.g. $F_{12}\sigma_1\sigma_2$, play an important role in the determination of the failure load.
7. The sign and magnitude of the individual stress components leads to a shift in the location of the failure point.

From the above observations it can be concluded that the discrepancy in the obtained value of the failure load can be significant if the error in the solution is not controlled. Further, the local stress values lead to varying contribution of the stress components to the failure index. Due to this, the initial point is no longer the initiation point for failure. Note that the failure point for the adapted mesh lies in the vicinity of the initial point. Hence, for the final failure load, the failure index at the initial point is close to one.

In order to account for this shift in the location of the failure point (possibly due to the mesh and the model), it is more useful to demarcate the failure regions, for example, the region for which the failure index is greater than 0.8. Such a region is shown in Fig. 11 with gray shading. Adaptivity can then be done with respect to the error in the average values of $\sigma_{\max}$ (maximum contributor to FI_{TW}) in this region. From Fig. 11b, it can be noted that the size of the failure region shrinks as the mesh is refined (here adaptivity was done with respect to the region near the edge $y = 0$). This is because the boundary layer is resolved better with the refined mesh.

Remark. Calculation of failure load makes no sense for domains which have corner or edge singularities, i.e. points where stresses are infinite. This is true for domains with re-entrant corners, change in boundary conditions. When the solution has such singularities, the adaptive mesh will give suitable refinements near the singular points, leading to large stresses at these points. This will cause the failure point to shift to the singular point, and the computed failure load will decrease monotonically with mesh refinement. In the examples considered in this study, this shift was not observed.

7. Conclusions

A comprehensive study of the point-wise quality of the stress components, obtained using various plate models, has been done for laminated plates under transverse loading. The issue of accurate computation of first-ply failure load has also been studied. From this study it can be concluded that

1. The point-wise displacement obtained using the HSDT and hierarchic models are not very accurate for thick laminates. The accuracy improves as the plate becomes thinner. This is because of the more pronounced shear effects in thicker laminates, leading to a piecewise higher-order polynomial behavior of the exact solution. The layerwise theory accurately captures this behavior for all cases.
2. The HSDT and hierarchic models are more reliable for thin plates while for thicker plates these models can give significant errors.
3. The layerwise model accurately captures the local state of stress for all laminated composite plates, for different plate thicknesses.
4. The in-plane stress components computed by all the models are accurate, for almost all the cases.
5. The transverse stress components computed by direct use of finite element data for layerwise model are in good agreement with exact one.
6. The transverse stress components computed by direct use of finite element data for HSDT and hierarchic models are significantly different, qualitatively and quantitatively. The equilibrium approach of post-processing gives more accurate transverse stress terms, for both symmetric and antisymmetric laminates.
7. Computed failure load is sensitive to the mesh, order of approximation and model used. Proper mesh design is necessary to ensure that local transverse stresses are computed accurately.
8. The primary contributors to the error in the computed failure load are the boundary layer, locking effect and discretisation error (as low order elements are used). Adaptivity resolves these and hence the failure load can go down by 40%. Hence, from design point of view, proper mesh design is essential.
9. Identification of failure zones (e.g. regions with $FI_{\mathrm{TW}} > 0.9$) may be a more useful information from design point of view.

References

[1] Reissner E. The effect of transverse shear deformation on bending of elastic plates. J Appl Mech 1945;12:A69–77.
[2] Mindlin RD. Influence of rotary inertia and shear on flexural motions of isotropic, elastic plates. J Appl Mech 1951;18:31–8.
[3] Reissner E. On the theory of bending of elastic plates. J Math Phys 1944;23:184–92.
[4] Reissner E. On bending of elastic plates. Quart Appl Math 1947;V(1):55–68.
[5] Reissner E, Stavsky Y. Bending and stretching of certain types of heterogeneous aeolotropic elastic plates. J Appl Mech, Trans ASME 1961;28(3):402–8.
[6] Whitney JM, Pagano NJ. Shear deformation in heterogeneous anisotropic plates. J Appl Mech, Trans ASME 1970;37:1031–6.
[7] Whitney JM. Shear correction factors for orthotropic laminates under static load. J Appl Mech, Trans ASME 1973;40:302–4.
[8] Whitney JM, Sun CT. A higher order theory for extentional motion of laminated composites. J Sound Vibr 1973;30(1):85–97.

[9] Lo KH, Christensen RM, Wu EM. A higher-order theory of plate deformation. Part 1. Homogeneous plates. J Appl Mech, Trans ASME 1977;44:663–8.
[10] Lo KH, Christensen RM, Wu EM. A higher-order theory of plate deformation. Part 2. Laminated plates. J Appl Mech, Trans ASME 1977;44:669–76.
[11] Reddy JN. A simple higher order theory for laminated composite plates. J Appl Mech, Trans ASME 1984;51:745–52.
[12] Szabó BA, Sharmann GJ. Hierarchic plate and shell models based on *p*-extension. Int J Numer Meth Eng 1988;26:1855–81.
[13] Babuška I, Szabó BA, Actis RL. Hierarchic models for laminated composites. Int J Numer Meth Eng 1992;33:503–35.
[14] Actis RL, Szabó BA, Schwab C. Hierarchic models for laminated plates and shells. Comput Meth Appl Mech Eng 1999;172:79–107.
[15] Srinivas S. A refined analysis of composite laminates. J Sound Vibr 1973;30(4):495–507.
[16] Di Sciuva M. An improved shear-deformation theory of moderately thick multilayered anisotropic shells and plates. J Appl Mech, Trans ASME 1987;54:589–96.
[17] Di Sciuva M. Development of an anisotropic, multilayered, shear-deformable rectangular plate element. Comput Struct 1985;21: 789–96.
[18] Toledano A, Murakami H. A composite plate theory for arbitrary laminate configurations. J Appl Mech, Trans ASME 1987;54: 181–9.
[19] Reissner E. On a certain mixed variational theories and a proposed application. Int J Numer Meth Eng 1984;20:1366–8.
[20] Bhaskar K, Vardan TK. Refinement of higher-order laminated plate theories. AIAA J 1989;27(12):1830–1.
[21] Barbero EJ, Reddy JN, Teply J. An accurate determination of stresses in thick laminates using a generalized plate theory. Int J Numer Meth Eng 1990;29:1–14.
[22] Ahmed NU, Basu PK. Higher-order finite element modeling of laminated composite plates. Int J Numer Meth Eng 1994;37: 123–9.
[23] Kapania RK, Raciti S. Recent advances in analysis of laminated beams and plates. Part I. Shear effects and buckling. AIAA J 1989;27(7):923–34.
[24] Ugrimov SV. Generalized theory of multilayer plates. Int J Solids Struct 2002;39:819–39.
[25] Han H, Kellogg RB. Differentiability properties of solutions of the equation $-\varepsilon^2\Delta u + ru = f(x,y)$ in a square. SIAM J Math Anal 1990;21(2):394–408.
[26] Arnold DN, Falk RS. A uniformly accurate finite element method for the Reissner–Mindlin plate. SIAM J Numer Anal 1989;26(6): 1290–726.
[27] Babuška I, Li L. The *h–p* version of the finite element method in the plate modelling problem. Commun Appl Numer Meth 1992;8: 17–26.
[28] Babuška I, Schwab C. A posteriori error estimation for hierarchic models of elliptic boundary value problems on thin domains. SIAM J Numer Anal 1996;23(1):221–46.
[29] Schwab C, Suri M, Xenophontos C. The *hp* finite element method for problems in mechanics with boundary layers. Seminar für Angewandte Mathematik Eidgenössische Technische Hochschule CH-8092 Zürich Switzerland. Research Report No. 96-20, October 1996.
[30] Hakula H, Leino Y, Pitkäranta J. Scale resolution, locking, and high-order finite element modelling of shells. Comput Meth Appl Mech Eng 1996;133:157–82.
[31] Schwab C. A-posteriori modeling error estimation for hierarchic plate model. Numer Math 1996;74:221–59.
[32] Zienkiewicz OC, Zhu JZ. A simple error estimator and the adaptive procedure for practical engineering analysis. Int J Numer Meth Eng 1987;24:337–57.
[33] Ladevèze P, Pelle JP, Rougeot PH. Error estimation and mesh optimization for classical finite elements. Eng Comput 1991;8: 69–80.
[34] Babuška I, Strouboulis T, Mathur A, Upadhyay CS. Pollution error in the *h* version of the finite element method and the local quality of a-posteriori error estimators. Finite Element Anal Des 1994;17: 273–321.
[35] Mohite PM, Upadhyay CS. Local quality of smoothening based a-posteriori error estimators for laminated plates under transverse loading. Comput Struct 2002;80(18–19):1477–88.
[36] Mohite PM, Upadhyay CS. Focussed adaptivity for laminated plates. Comput Struct 2003;81:287–93.
[37] Pagano NJ. Exact solutions for rectangular bi-directional composite sandwich plates. J Compos Mater 1970;4(1):20–35.
[38] Pagano NJ, Hatfield SJ. Elastic behavior of multilayered bidirectional composites. AIAA J 1972;10(7):931–3.
[39] Pagano NJ. Exact solutions for composite laminates in cylindrical bending. J Compos Mater 1969;3:398–411.
[40] Pagano NJ. Influence of shear coupling in cylindrical bending of anisotropic laminates. J Compos Mater 1970;4:330–43.
[41] Tsai SW, Wu EM. A general theory of strength for anisotropic materials. J Compos Mater 1971;5:55–80.
[42] Reddy YSN, Reddy JN. Linear and non-linear failure analysis of composite laminates with transverse shear. Compos Sci Technol 1992;44:227–55.